

# 1 **Effects of naval traffic on sediment erosion and accumulation in ports: a new model-based methodology**

2 *Antonio Guarnieri*<sup>(1)</sup>, *Sina Saremi*<sup>(2)</sup>, *Andrea Pedroncini*<sup>(3)</sup>, *Jacob H. Jensen*<sup>(2)</sup>, *Silvia Torretta*<sup>(3)</sup>, *Marco Vaccari*<sup>(4)</sup>,  
3 *Caterina Vincenzi*<sup>(4)</sup>

4 *(1) Istituto Nazionale di Geofisica e Vulcanologia, Sezione di Bologna, Via D. Creti, 12, 40128 Bologna, Italy*

5 *(2) DHI, Horsholm, Denmark*

6 *(3) DHI S.r.l., Via Bombrini 11/12, 16149 Genova*

7 *(4) Autorità di Sistema Portuale del Mar Ligure Occidentale (Genova), Palazzo San Giorgio - Via della Mercanzia 2*

8 *Corresponding author: Antonio Guarnieri; antonio.guarnieri@ingv.it*

## 9 **Abstract**

10 The action of propeller-induced jets on the seabed of ports can cause erosion and the deposition of sediment around  
11 the port basin, potentially significantly impacting on the bottom topography over the medium and long time. If such  
12 dynamics are constantly repeated for long periods, a drastic reduction in ships' clearance can result through accretion,  
13 or it can threaten the stability and duration of structures through erosion. These sediment-related processes present  
14 port managing authorities with problems, both in terms of navigation safety and in the optimization of management  
15 and maintenance activities of the ports' bottom and infrastructures.

16 In this study, which is based on integrated numerical modeling, we examine the hydrodynamics and the related  
17 bottom sediment erosion and accumulation patterns induced by the action of vessel propellers in the passenger port of  
18 Genoa (Italy). The proposed new methodology offers a state-of-the-art science-based tool that can be used to  
19 optimize and efficiently plan port management and seabed maintenance.

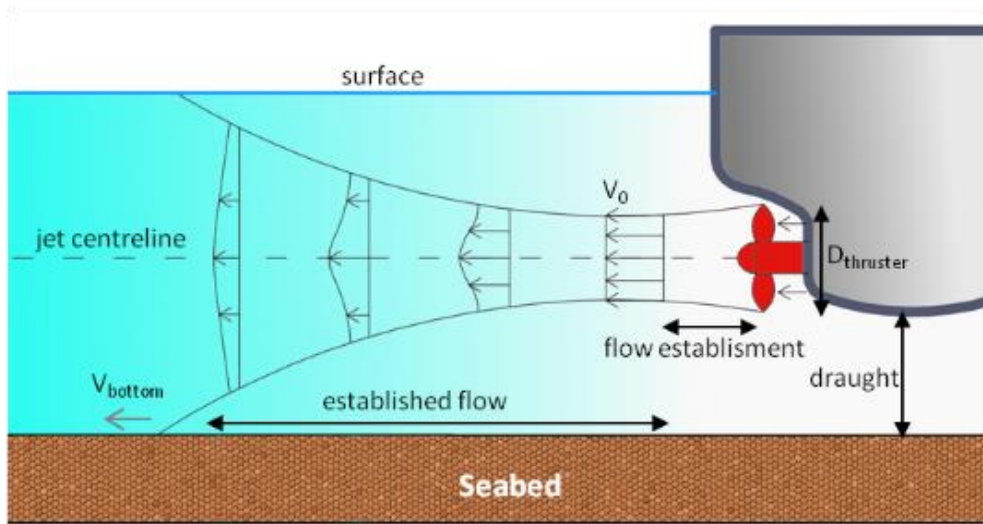
20

## 21 **1 - Introduction**

22 The operational activities of harbors and ports are closely related to the local bathymetry, which must be sufficiently  
23 deep to guarantee the regular passage, maneuvering and berthing of ships. However, ship clearance is often so limited  
24 that it threatens the safety of in-port navigation, and ships may even hit the seabed in extreme cases. This is therefore  
25 a source of criticalities that often result in management and maintenance efficiency problems in terms of the bottom  
26 and a port's infrastructure in general (Mujal-Colilles et al., 2016; Castells-Sanabra et al., 2020).

27 The action of a ship's main propellers means that traffic in ports is responsible for generating intense current jets, as  
28 noted in Figure 1. Figure 1 The high velocities induce shear stresses on the sea bottom, which can possibly result in

29 sediment resuspension when they exceed the critical stress point for erosion (Van Rijn, 2007, Soulsby et al., 1994;  
 30 Grant and Madsen, 1979). Before depositing back onto the sea floor the re-suspended sediment may be transported  
 31 widely around the basin by the combined effects of natural currents such as those induced by tides, winds or density  
 32 gradients, and by vessel-related currents, such as those induced by the propellers or the movement and displacement  
 33 of ships. The continuous traffic in and out ports can thus result in the displacement of a huge volume of seabed  
 34 material, which can then induce significant variations in the bathymetry over medium to long time scales. The  
 35 formation of erosional or depositional trends in specific areas of port basins can potentially result from these  
 36 variations.



37  
 38 **Figure 1 - Example of propeller induced jet of a moving ship (main propulsion without rudder)**

39 If such dynamics are particularly pronounced and rapid (bottom accretion of an order of tens of centimeters per year  
 40 or even higher), the port authorities must undergo dredging operations for the maintenance of the seabed, to fully  
 41 recover the clearance and ensure the conditions necessary for undisturbed ships motion, maneuvering and  
 42 docking/undocking operations.

43 Most of the published literature about the effects of ships' propellers on port sediments and structures is experimental,  
 44 and is mainly conducted in laboratories using physical models ( Mujal-Colilles et al. 2018; Yuksel et al. 2019). Few  
 45 practical instruments are available for port authorities that can provide robust and scientifically based analyses and  
 46 predictions of the relevant processes. Such tools can enable them to plan specific actions aimed at maintaining the  
 47 seabed, and thus help both guarantee the continuity of operational activities of ports and optimize the use of economic  
 48 resources. Unplanned maintenance activities usually involve additional costs due to the need to operate in emergency  
 49 conditions and in some cases partially interrupt the service.

50 The integrated numerical modeling of hydrodynamics and sediment transport represents an important aid to port

51 authorities, and more broadly to port managers and operators, as suggested by Mujal-Colilles (2018). This can  
52 reproduce and thus provide a better understanding of the seabed sediment dynamics induced by ships' propellers over  
53 short, medium and long time scales, thus establishing what tools are required to ensure the efficient operational  
54 maintenance of the seabed.

55 Propeller induced jets have mainly been studied using empirical formulas based on specific characteristics of the ships  
56 and ports of interest, such as the bathymetry, propeller typology, diameter and rotation rate, and ship's draught. The  
57 most common approaches are the German method (MarCorm WG, 2015; Grabe, et al., 2015; Abromeit et al., 2010,) and the Dutch method (CIRIA et al., 2007). The resulting induced velocities are usually only considered locally, to  
58 inform the technical design of mooring structures and the protection of a port's infrastructure. Although various  
59 assumptions are introduced through empirical formulas, these approaches are limited and do not fully consider the  
60 three-dimensional evolution of the induced jet throughout the water column at any distance from the propeller, or at  
61 any location of the port. These tools are therefore not suitable for the comprehensive management of ports.

62 We conduct a pilot study of the hydrodynamics and seabed evolution induced by ships' propellers in the passenger  
63 area of the Port of Genoa (Figure 2Figure 2), where the naval traffic involves mainly passenger vessels (ferries and  
64 cruise ships, generally self-propelled) and in which the resulting sediment dynamics in terms of erosion/deposition  
65 rates are particularly significant: estimated in the order of several tens of centimeters per year (as directly estimated  
66 and communicated by the Port Operators and via an analysis of bathymetric surveys). In this study, we propose that  
67 the integrated high-resolution numerical modeling of three-dimensional hydrodynamics and sediment transport can be  
68 a robust and science-based tool for the optimization and efficient planning of port management and maintenance  
69 activities. We propose a new methodology that can be used in a delayed mode, and can thus reproduce the historical  
70 major sediment processes over time, as in this study, or in a prediction mode through the potential implementation of  
71 real-time operational services.

72 The remainder of this paper is organized as follows: in Sect. 2 we introduce our methodology, and the data available  
73 for the study are presented in Sect. 3. Sect. 4 describes the numerical models used, and the results of the numerical  
74 simulations are presented and discussed in Sect. 5. Finally, the summary and conclusions of the work are given in  
75 Sect. 6.

76

## 77 **2 – Methods**

78 The study is based on the latest versions of the hydrodynamic and mud transport models MIKE 3 FM (DHI, 2017),  
79 which are described in detail in Sect. 3 and in APPENDICES A1 and A2. A very high resolution was used in the  
80 numerical model to realistically reproduce the propeller induced jet, both in the vertical and in the horizontal, at  
81

82 approximately 1-2 meters and 5 meters, respectively. Together with a non-hydrostatic version of the hydrodynamic  
83 model, this enables the processes and dominant patterns of the current field generated by the ships propellers during  
84 the navigation and maneuvering inside the port to be reproduced very accurately.

85 As shown in Figure 2 Figure 2, 12 docks have been included in the study (marked with orange or red lines indicating  
86 ferry or cruise vessels, respectively). The Port Authority mainly focused on passenger vessels as they considered their  
87 effect on the seabed to be greater than other types of vessels that have much less frequent passage. Moreover,  
88 passenger ships are in general self-propelled, while other vessel types are often driven by tugboats. We therefore only  
89 simulated passenger ships.

90 The turning basins in which arriving vessels undergo maneuvers for berthing are represented in Figure 2 Figure 2 by  
91 the white-dashed circles marked *a* and *b*. Circle *a* refers to vessels berthing at docks T5 to T11, while circle *b* refers to  
92 vessels for docks T1 to T3. Finally, the turning area for vessels arriving at docks D.L., 1012 and 1003 is at the  
93 entrance of the port and is not simulated in this study, as it is out of our area of interest.

94 The general methodology can be separated into the following phases.

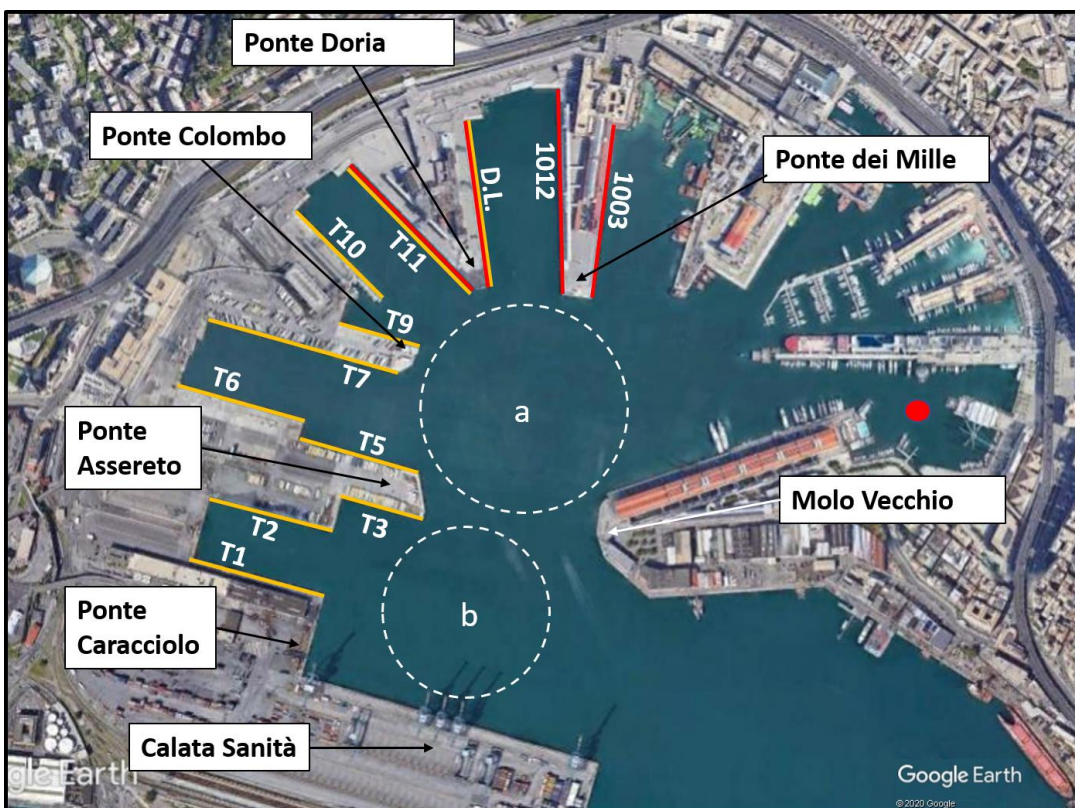
- 95 1. *Assessment of the naval traffic during a typical year.* This phase is fundamental, as it identifies the typical  
96 dynamics of the naval traffic in the different sectors of the port and the characteristics of the ships that have  
97 the greatest effect on the hydrodynamics and sediment re-suspension on the bottom. These include the size of  
98 the ships, the related draught, the dimension of the propellers and their typical rotation rates. The results of  
99 the analysis, which are discussed in detail in Sect. 4.1, also enabled representative synthetic vessels for each  
100 berth of the port to be defined.
- 101 2. *Implementation of a high-resolution 3D hydrodynamic model of the port of Genoa.* This numerical  
102 hydrodynamic model considered ship routes, both entering and exiting the port, as established through the  
103 previous vessel traffic analysis phase. As detailed in Sect. 4.1, 24 simulations of the hydrodynamic model  
104 have been implemented, one for each dock and route considered (docking and undocking). The resulting 24  
105 scenarios were then simulated separately. This enabled us to analyze the effect of each vessel's passage on  
106 the induced hydrodynamics of the basin. Each hydrodynamic contribution was then used to drive the  
107 sediment transport model. This approach does not consider potential simultaneous interactions amongst  
108 hydrodynamic patterns generated by different propellers, as we assume that vessels are unlikely to pass each  
109 other very closely.
- 110 3. *Implementation of a coupled sediment transport model.* Based on the available data, a numerical model of  
111 sediment resuspension and transport for fine-grained and cohesive material was then implemented. The

112 model was combined with the hydrodynamics resulting from the 24 different vessels scenarios. The  
113 simulations of the sediment model were conducted separately for the hydrodynamic component.

114 4. *Collating the results and the overall analysis.* The effects of the passage of the single vessels on the bottom  
115 sediment were then combined in terms of the erosion/deposition resulting from the overall number of  
116 passages over the analyzed one-year period of time. This enabled us to provide aggregated information on  
117 the annual sediment dynamics.

118 We then conducted a semi-quantitative calibration/validation of the modeling results through a comparison of the  
119 seabed evolution reproduced using the integrated modeling system and the various bathymetric maps derived from  
120 surveys of the port topography at approximately one year intervals.

121 The proposed approach assumes that each hydrodynamic and sediment transport simulation uses the same bathymetry  
122 as the initial bottom condition. Although this assumption may have implications, as we explain in the results section,  
123 it does not compromise the main conclusions of the study.



124  
125 **Figure 2 - Passenger port of Genoa.** The colored lines along the docks refer to the typology of the operating  
126 ships: red lines indicate cruise vessels while orange lines indicate ferries. The names of the docks (in white)  
127 are next to the colored lines are. The red dot represents the location of the station where sediment samples with  
128 physical information on the grains are available (see Sect. 4.2). The white dashed circles marked as *a* and *b*  
129 represent the turning areas for vessels berthing to docks T5 to T11 and to T1 to T3

130

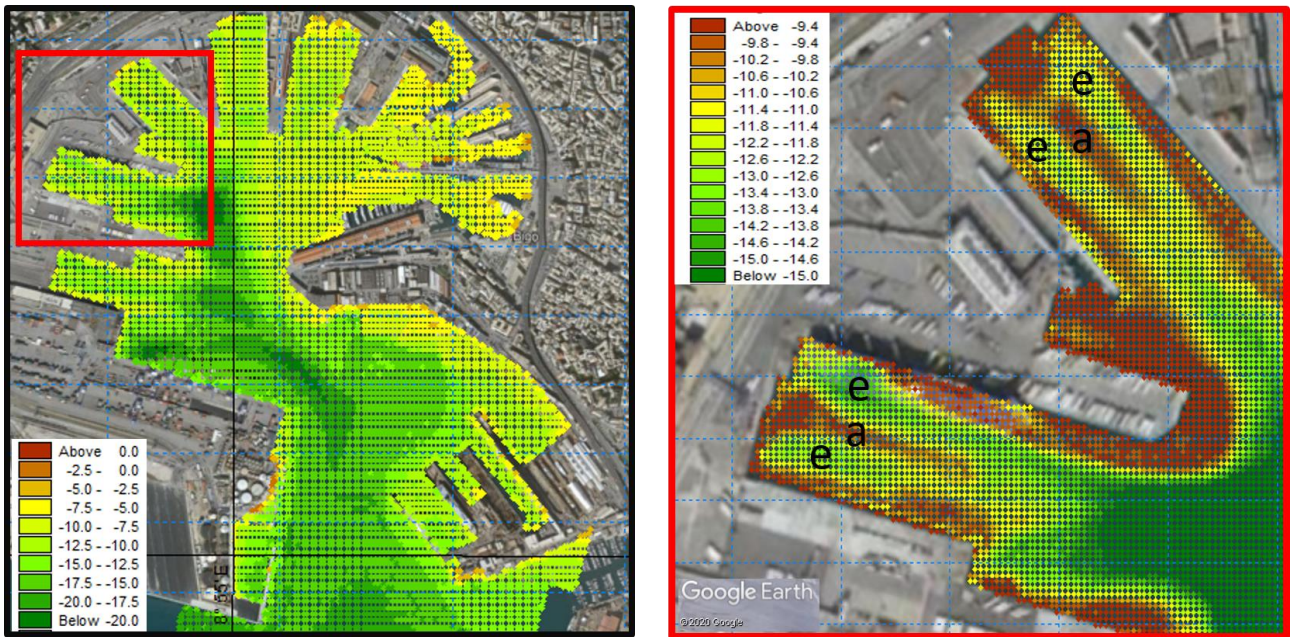
### 131 **3 – Available data and information**

132 Most of the data necessary for this project were provided by the Port Authority of Genoa and Stazioni Marittime SpA,  
133 the main port operator in the area.

134

#### 135 **3.1 – Bathymetry**

136 Several bathymetry surveys of the sectors of the port were available at various resolutions. The dataset used for the  
137 simulations was obtained by merging the latest available surveys (March-June 2018) of the inner sectors of the port,  
138 delivered on a regular grid of five meters of resolution. Figure 3Figure 3 shows the merged bathymetry for the entire  
139 port (left panel) and for a detail of the Ponte Colombo and the surrounding basin. The main area of interest for the study  
140 (from the line between Calatà Sanità and Molo Vecchio to the end of the Port, see Figure 2) measures approximately  
141 0.60 km<sup>2</sup> and has an average depth of approximately 13 meters. The bathymetry is in general heterogeneous. The wet  
142 basins are approximately 10-11 meters deep, while areas shallower than 10 meters are present only in the eastern part of  
143 the basin, where yachts and non-commercial vessels operate. A deep natural pit is clearly visible a few tens of meters  
144 off the right edge of *Ponte Colombo* and *Ponte Assereto*, extending approximately 22 meters below the water surface.  
145 The Port Authority has regarded this area as a preferred site for dumping the sediment resulting from regular  
146 maintenance dredging operations of the seabed, in sectors where depositional trends are large enough to reduce vessels  
147 clearance and to affect the safety of navigation inside the port. This depressed area is also used as a turning area by  
148 passenger ferries heading to docks T5, T6, T7 and T9, which cover approximately 50% of the naval traffic in the basin  
149 (see Sect. 4.1). During their manoeuvres over this pit the turning ferries produce intense turbulence, which may reach  
150 the newly dumped material resulting from the dredging operations. This material is still loose and can consequently be  
151 easily re-suspended and transported around the port basin, thus making the dredging operations ineffective.



152

153 **Figure 3 - Bathymetry of the port of Genoa. Entire Passenger Port (left panel) and zoom on *Ponte Colombo* and**  
 154 **the surrounding basins (from T5 to T11, right panel)**

155

156 The bathymetry presented in the right panel of Figure 3 follows the pattern of erosion and accumulation  
 157 common to wet basins confined among docks. The propeller activity when vessels leave or approach the berth induces  
 158 areas of erosion, identified by channels of deepened bathymetry (referred to with an “e” in the right panel of Figure  
 159 3 and coloured yellow-green) and areas of accumulation identified with tongues of shallower bathymetry  
 160 (denoted by “a” in the right panel of Figure 3, and coloured brown).

161 Another survey covering approximately the same area as that of Figure 3 is available for the period May-June  
 162 2017. By comparing the topographical information of the two and integrating the information on dredging activities  
 163 during the same period, we were able to reconstruct in a semi-quantitative fashion the sediment dynamics occurring  
 164 during this time window of approximately one year. This information was then used in the calibration/validation  
 165 process for the numerical model of sediment erosion and transport, as detailed in Sect. 5.

166

167 **3.2 – Sediment data**

168 The availability of information on sediment textures in the sea is limited. We were able to access the MARine Coastal  
 169 Information sySTEM (MACISTE; <http://www.apge.macisteweb.com>) implemented by the Department of Science of  
 170 Earth, Environment and Life (DISTAV) of the University of Genova, where the results of several chemical and physical  
 171 sediment surveys are stored and are accessible. Unfortunately, although the chemical information is comprehensive,

172 information on grain size for the inner area of the port is incomplete. The red dot of Figure 2Figure 2 represents the  
173 only location inside the basin where information on the texture composition and grain size was available. These  
174 characteristics are necessary for the sediment transport model and in the simulations for the entire domain of the  
175 numerical model (see Sect. 4.2).

176

### 177 **3.3 – Naval traffic**

178 In terms of naval traffic, 2017 was considered by the Port Authority of Genoa and Stazioni Marittime SpA to be a  
179 typical year. The traffic data were available on a daily basis and included information on the docks of arrival/departure  
180 and the names of the vessels involved. The entire year was considered, to account for the typical seasonality of the  
181 traffic concentration, which is particularly significant for passenger vessels from the end of spring to the beginning of  
182 fall.

183 The characteristics of the vessels required for the modelling activity (i.e., length, width, tonnage, draught) were  
184 obtained from information available through public sources. The outcomes of the analysis are presented in Sect. 4.1.

185

## 186 **4 – The numerical models**

187 The non-hydrostatic version of the MIKE 3 HD flow model (DHI, 2017) was used to simulate the propeller induced  
188 three-dimensional current along the port basin. The resulting hydrodynamic field was coupled with the sediment  
189 transport module MIKE 3 MT (DHI, 2019), suitable for fine-grained and cohesive material, in order to drive the  
190 erosion, advection-dispersion and deposition of fine sediment along the water column.

191

### 192 **4.1 – The hydrodynamic model**

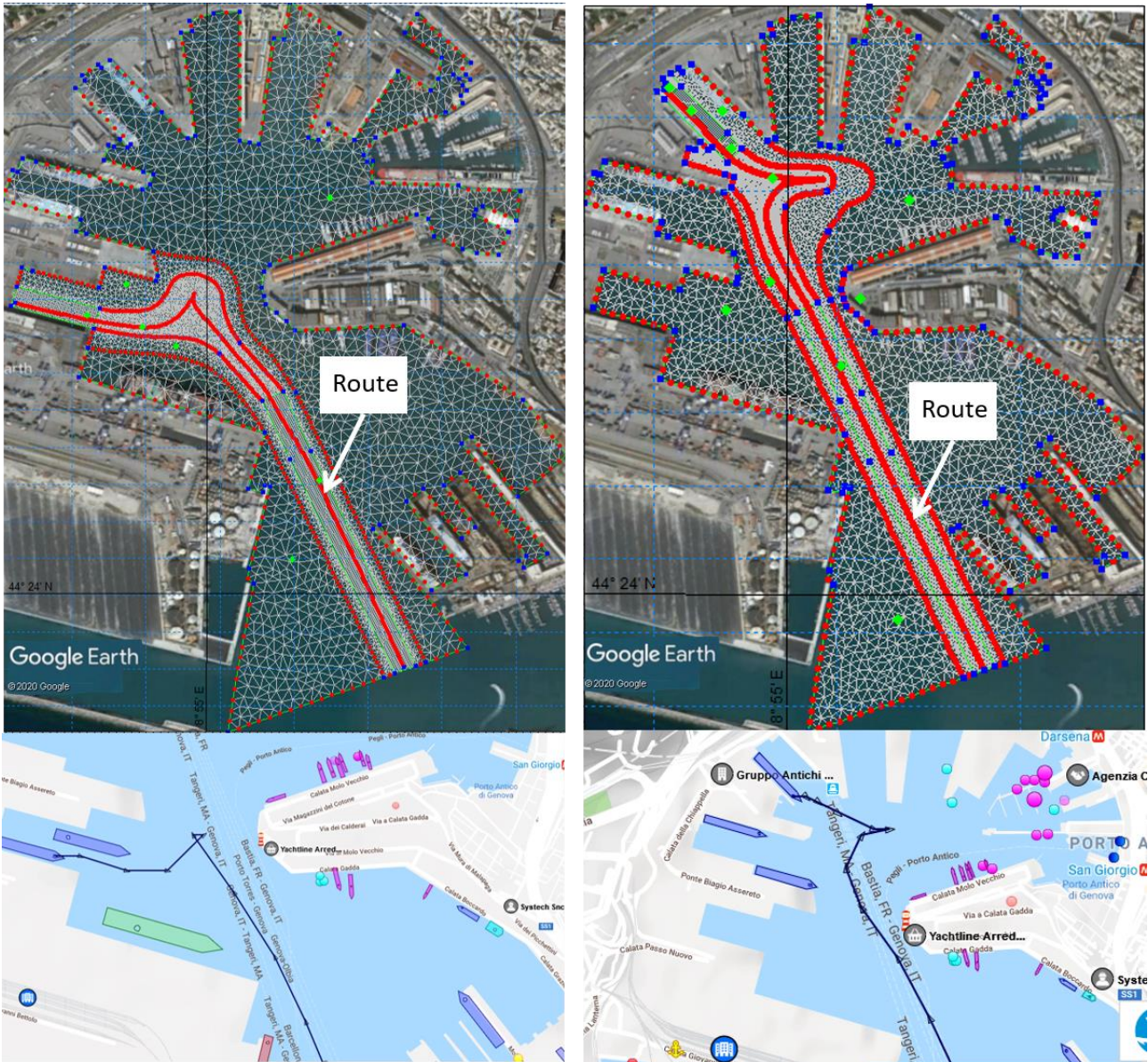
193 The MIKE 3 FM flow model is an ocean circulation model suitable for different applications within oceanographic,  
194 coastal and estuarine environments at global, regional and coastal scales. It is based on the numerical solution of the  
195 Navier-Stokes equations for an incompressible fluid in the three dimensions (momentum and continuity equations),  
196 based on the advection-diffusion of potential temperature and salinity and on the pressure equation, which in the present  
197 non-hydrostatic version is split into hydrostatic and non-hydrostatic components. The closure of the model is obtained  
198 by the choice of a turbulence closure formulation with various possible options within a constant value, and a  
199 logarithmic law scheme or a k- $\epsilon$  scheme, which is used in the present implementation. The surface is free to move and it  
200 can be solved using a sigma coordinate (as used in the present study) or a combined sigma-zed approach. The spatial  
201 discretization of the governing equations of the model follows a cell-centred finite volume method. In our



202 implementation of the model we used the barotropic density mode, and thus temperature, salinity and consequently  
203 density were constant in time and space during the simulations.

204 The domain of the present implementation of the model is presented in the upper panels of Figure 4Figure 4. The  
205 images show two examples of computational grids used for the simulations. Here, the docks are T1 (left panel) and T10  
206 (right panel) during inbound operations. The grids are a combination of unstructured triangular and quadrilateral cells  
207 with horizontal resolutions varying from 30 meters in the furthest areas from the ship trajectory to 5 meters  
208 approximately within the closest area to the ships' propellers. The mesh is rectangular in areas where the ships are  
209 moving straight ahead and the 5 meter resolution covers a corridor of approximately 50 meters of width. In the  
210 manoeuvring areas, the mesh becomes unstructured and the resolution is again 5 meters. The red lines in the middle of  
211 the five-meter resolution corridors of the upper panels represent the routes followed by the ships inside the port. The  
212 lower panels of the figure are snapshots taken from the web service <https://www.marinetraffic.com>, which show the  
213 actual routes of the vessels birthing in the docks in the upper panels (T1 and T10) as recorded by the AIS system  
214 mounted on the ships. As shown in Figure 4Figure 4 the reconstructed trajectories of the ships in the model are  
215 realistic and fully representative of the real trajectories.

216 Table 1 Table 1 shows the results of the traffic analysis within the Port of Genoa for 2017 conducted using the daily  
217 traffic data provided by Stazioni Marittime SpA. The annual traffic is generally regular, and its frequency varies from  
218 basin to basin and depends on the season. Generally, the busiest docks are T5, T6 and T7, accounting for almost 50% of  
219 the total traffic. They follow an approximately daily frequency all year round, whereas the wet basins towards the end  
220 of the port, which mainly serve cruise vessels, show an evident seasonality, probably related to the Mediterranean cruise  
221 season (few and irregular passages from January to May, then regular and in a much increased frequency from June to  
222 October/November).



223

224 **Figure 4 - Model domain and computational grids for docking routes of T1 (left panel) and T10 (right panel)**

225 **docks. In the lower panels the corresponding actual routes are shown**

226

227 **Table 1 - Analysis of ship traffic in the port of Genoa for year 2017 and main characteristics of the ship**

228 **representative of each dock. The ship's length, width, draught and propeller's diameter values are expressed in**

229 **meters**

Dock	Number of Berthing	% Berthing	Average Length [m]	Average Width [m]	Average Draught [m]	Average Diameter [m]
1012	122	6.4%	318.41	37.86	8.33	5.80
1003	47	2.5%	276.20	30.07	7.45	5.20
D.L.	12	0.6%	290.86	32.02	7.82	5.40
T11	123	6.4%	213.23	31.67	7.16	5.20
T10	202	10.5%	181.88	26.44	6.46	4.70
T9	8	0.4%	152.96	24.81	5.91	4.40
T7	308	16.1%	214.27	26.45	6.85	4.90

<b>T6</b>	291	15.2%	204.93	26.35	6.62	4.80
<b>T5</b>	351	18.3%	203.93	29.57	6.95	5.00
<b>T3</b>	87	4.5%	155.16	25.60	6.17	4.50
<b>T2</b>	202	10.5%	185.66	27.85	6.68	4.80
<b>T1</b>	164	8.6%	204.00	28.33	6.93	5.00
<b>TOTALE</b>	<b>1917</b>	100.0%	---	---	---	

230

231 In the vertical, the model is resolved over 10 evenly distributed sigma layers. The resulting layer depths vary from  
 232 approximately 1 meter in the berthing areas to approximately 2 meters in the pits and in the areas closer to the port's  
 233 entrance.

#### 234 4.1.1 - Propeller jet velocity

235 The propellers' maximum jet velocity was calculated based on the Code of Practice of the Federal Waterways  
 236 Engineering and Research Institute (Abromeit et al., 2010) and the PIANC Report n. 180 (MarCom WG 180, 2015),  
 237 taking the German approach. The relevant parameters for the calculations are shown in Figure 1Figure 1. The  
 238 maximum velocity  $V_0$  after the jet contraction generated by the propeller is developed along its axis. For unducted  
 239 propellers, we use Eq. (1a) for the propeller ratio  $J=0$  (ship not moving) or Eq. (1b) for  $J \neq 0$  (moving ship).

240

$$241 \quad V_0 = 1.60 f_n n_d D \sqrt{K_T} \quad (1a)$$

$$242 \quad V_{0j} = \frac{\sqrt{(J^2 + 2.55 K_{Tj})}}{\sqrt{1.4 \frac{P}{D}}} V_0 \quad (1b)$$

243 where  $n_d$  [1/s] is the design rotation rate of the propeller;  $f_n$  is the factor for the applicable propeller rotation rate (non-  
 244 dimensional);  $D$  is the propeller diameter [m];  $K_t$  or  $K_{tj}$  is the thrust coefficient of the propeller (non-dimensional) in the  
 245 case of non-motion or motion of the ship, respectively; and  $P$  is the design pitch [m]. Typical values for  $f_n$  are 0.7 - 0.8  
 246 during manoeuvring activities, while the  $P/D$  ratio can be assumed to be approximately equal to 0.7.  $K_t$  or  $K_{tj}$  can be  
 247 estimated through Eq. (2a) and (2b), according to the state of motion of the ship:

$$248 \quad K_t = 0.55 \frac{P}{D} \quad (2a)$$

$$249 \quad K_{tj} = 0.55 \frac{P}{D} - 0.46J \quad (2b)$$

250 The propeller ratio  $J$  depends on a wake factor  $w$ , which varies from 0.20 to 0.45 (non-dimensional), and on the velocity  
 251 of the ship according to Eq. (3):

$$252 \quad J = \frac{v_s(1-w)}{nD} \quad (3)$$

253 As proposed by Hamill (1987) and further described by Wei-Haur Lam et al. (2005), the downstream propeller-induced  
254 jet is divided into a zone of flow establishment (closer to the propeller) and a zone of established flow (further  
255 downstream). The resulting velocity  $V_0$  used in the model to calculate the corresponding discharge and momentum  
256 sources is considered as the maximum velocity at the beginning of the zone of the established flow.

257 As we had no direct information about the size of the ship's propellers, we referred to the specific literature. For the  
258 propellers of the Ro-Ro ferries that typically serve docks T1, T2, T3, T5, T6, T7, T9, T10 and T11, we referred to the  
259 report n° 02 of the project "Mitigating and reversing the side-effects of environmental legislation on Ro-Ro shipping in  
260 Northern Europe" (Kristensen, 2016) implemented by the Technical University of Denmark (DTU) and HOK  
261 Marineconsult ApS. According to this study, the relationship between the draught and the diameter of the ferry's  
262 propeller is given by Eq. (4):

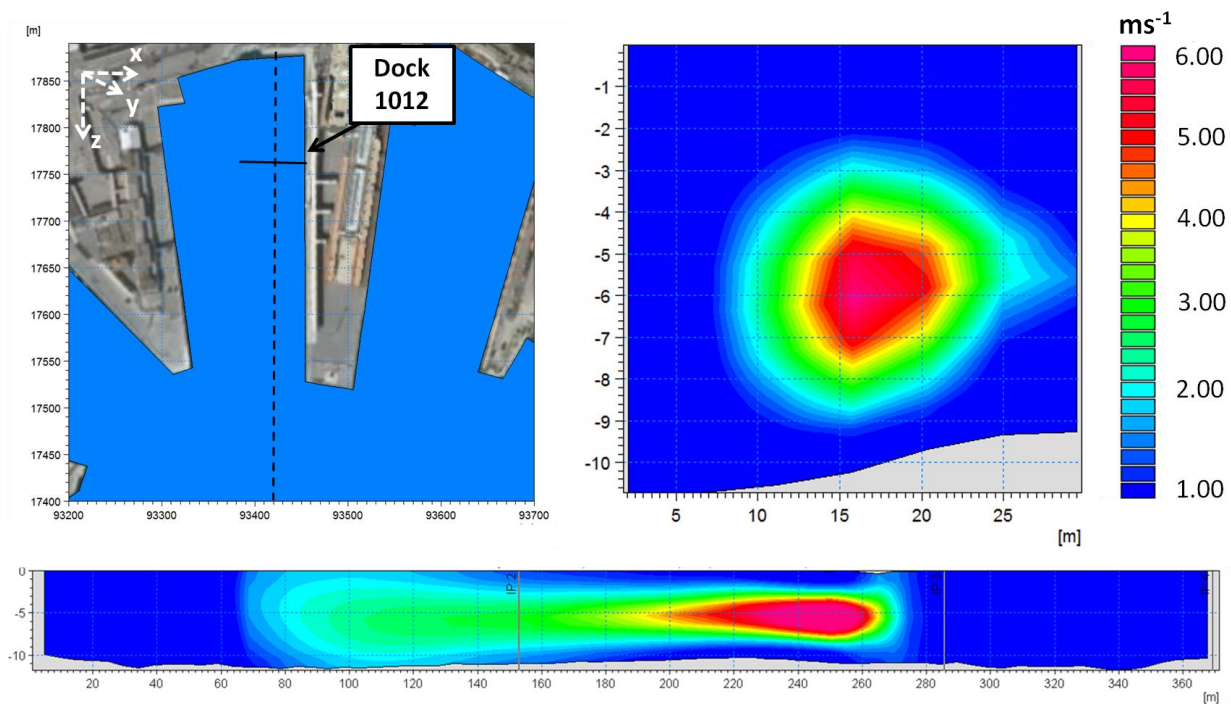
$$263 \quad D_{prop} = 0.56 \times H_{draught} + 1.07 \quad (4)$$

264  
265 where  $D_{prop}$  is the propeller's diameter [m], and  $H_{draught}$  is the maximum draft of the ship [m]. This relation is not valid  
266 for cruise ships, as they typically have larger propellers. For this type of ship, which serve docks 1012, 1002 and  
267 partially D.L. and T11, we directly referenced operators in the passenger ship design sector, and double checked the  
268 information with the formulas from Eq. (4) and from Eq. (5), which is also valid for double propeller passenger ships.  
269 This qualitative analysis provided the diameters presented in Table 1 Table 1.

$$270 \quad D_{prop} = 0.85 \times H_{draft} - 0.69 \quad (5)$$

271 The water discharge was obtained by combining the diameter of the propeller and the intensity of the jet, which was  
272 discretized into a certain number of smaller discharges associated with various smaller sources of momentum in the  
273 numerical model. We thus realistically represented the propeller. The distribution of volume and momentum sources  
274 follows a spatially Gaussian (normal) distribution with a discretization step of 0.5 meters and a constant rotation rate of  
275 the propeller.

276 Figure 5 Figure 5 shows the propeller's induced jet in the hydrodynamic model. The left panel represents the plan of  
277 Dock 1012, where a large cruise ship is departing. The solid line of the upper left panel is the location of the vertical  
278 transect shown in the upper right image, representing the jet velocity in the plane  $xz$ . The dashed line in the upper left  
279 panel represents the trajectory followed by the axis of the departing ship, and the associated jet's velocity in the  $yz$  plane  
280 is shown in the bottom panel. Although the horizontal resolution is non-optimal in terms of propeller representation, the  
281 resulting jet appears extremely realistic both in transverse and longitudinal directions.

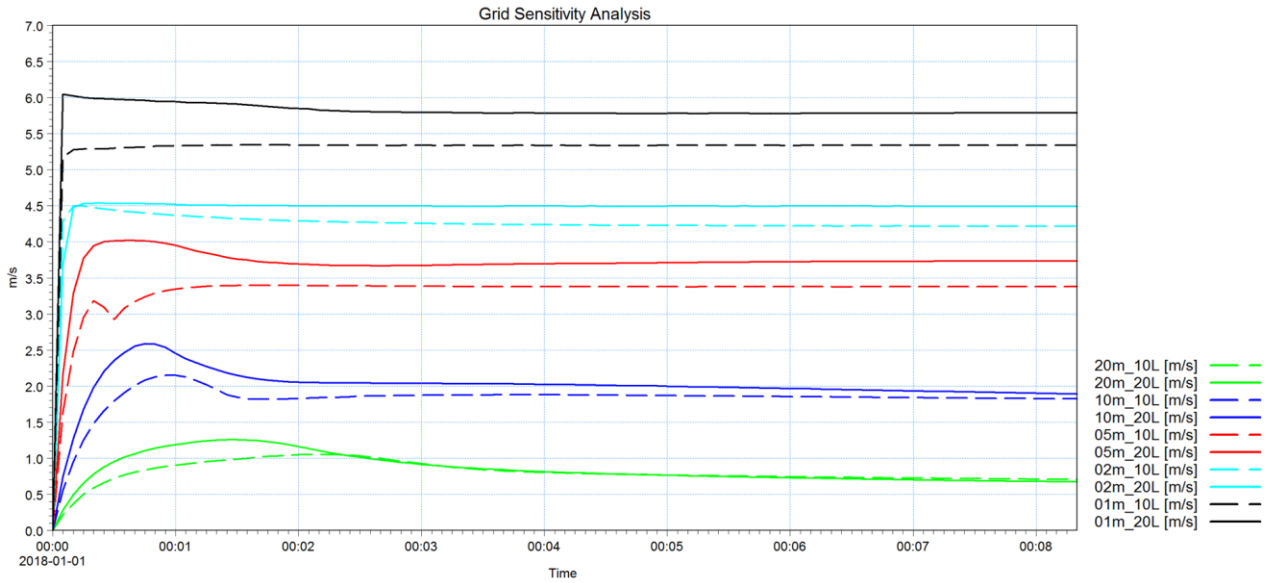


282 **Figure 5 – Representation of the propeller-induced jet of the most representative ship departing from Dock 1012.**  
 283

284 **Left: plan view; the dashed line represents the trajectory followed by the axis of the undocking ship, the solid**  
 285 **line represents the position of the vertical transect shown in the upper right panel, showing the jet’s induced**  
 286 **velocity in the xz plane (propeller’s plane). Lower panel: transect of velocity along the propellers axis (yz plane).**  
 287 **Velocities are in ms<sup>-1</sup>**

288 To preserve the water mass budget, we associated a sink to each source. Sinks are prescribed in terms of negative  
 289 equivalent discharge ( $\text{m}^3\text{s}^{-1}$ ) in the grid cell adjacent to that hosting the source, in the direction of the ship motion (sinks  
 290 precede corresponding sources).

291 The choice of the vertical and horizontal resolutions of the hydrodynamic model were the result of a thorough  
 292 sensitivity analysis of the grid’s cell dimensions. We assumed that the most appropriate resolution for the model allows  
 293 the maximum (jet centreline) current produced by the combined discharge and momentum sources in the model to reach  
 294 the input maximum velocity of  $V_0$ . For the sensitivity analysis, we considered a 4-meter diameter propeller with a  
 295 rotation rate of two rounds per second (rps) at full power. According to Eq. (1b), this configuration results in a  $V_0$  of  
 296 approximately  $6 \text{ ms}^{-1}$  at the depth of the propeller’s axis once the jet is fully developed. We set up an experimental  
 297 configuration domain 100 meters wide and 500 meters long. We tested horizontal resolutions of 20 m, 10 m, 5 m, 2 m  
 298 and 1 m, while for the vertical we considered two configurations: 10 and 20 layers in a constant bathymetry of 20  
 299 meters. The input value of the jet current to the model was  $6 \text{ ms}^{-1}$ .



300

301 **Figure 6 – Model grid sensitivity analysis to the cells dimension. The different colors correspond to the different**  
 302 **horizontal resolution. Dashed lines indicate the configurations with 10 layers while solid lines indicate those with**  
 303 **20 layers**

304 Figure 6 shows the sensitivity analysis of the grid resolution. The resulting velocity at the propeller’s axis is  
 305 proportional to the resolution, both in the vertical and the horizontal: the higher the resolution, the higher the resulting  
 306 velocity. The most appropriate grid is that with a 1-meter resolution and 20 vertical layers, which is the only  
 307 configuration of the model that allows the jet to reach the maximum speed imposed as the input. However, this  
 308 configuration would require approximately 1 year of computational time to run the 24 simulations implemented in this  
 309 study in the same computational configurations, which is obviously unrealistic. We thus sought a compromise between  
 310 acceptable computational demand and realistic resulting velocity. The final configuration took 5 meters as the  
 311 horizontal resolution and 10 vertical levels. As these resolutions did not allow for the complete development of the  
 312 current speed, we introduced a correction to the input velocity of each simulated vessel by increasing it by the necessary  
 313 amount to reach the empirically calculated  $V_0$ . This involved considerable additional time for manual calibration.

314 **4.1.2 – Forcing and boundary conditions**

315 Due to the nature of the focal processes, we only account for the force of the propellers of the vessels. The jet induced  
 316 by its motion is of an order of magnitude of several meters per second in the area surrounding the blades and when  
 317 unconstrained it has a length of influence of at least 40-50 times the propeller’s diameter behind the ship (Verhei, 1983).  
 318 This is also an important source of toe scouring in the presence of a quay wall (Hamill & Johnston 1999). Natural  
 319 forcing such as wind, density gradients or tides are one to two orders of magnitude smaller, and can thus be neglected  
 320 without introducing errors that can potentially affect sediment resuspension from the bottom. However, the Bernoulli  
 321 wake may be responsible for currents of comparable intensity (Rapaglia et al., 2016), although smaller, and can be a

322 forcing source in the system. Anyhow, we do not consider this due to technical complications and time constraints.  
323 Including such a process in further developments and analysing its impact on the overall dynamics of ship-induced  
324 sediment transport would be of interest. Our final results prove satisfactory, suggesting that the governing processes for  
325 these dynamics are associated more with propeller-induced currents than with the motion of the ship itself, likely due to  
326 the limited speeds of vessels in this inner part of the harbour and to the relatively large volume of water available for  
327 each passing vessel.

328 The boundaries of the hydrodynamic domain are the docks around the basin and the port entrance, which is the only  
329 open boundary. Here we imposed a Flather condition (1976) assuming constant zero velocities and levels. This allowed  
330 us to minimize the boundary effects, albeit with some interference between the flux and the boundary line (not shown).  
331 However, due to the distance between the open boundary line and the berthing areas, such effects do not influence the  
332 results of the study. A zero normal velocity was imposed along the closed boundaries.

333

#### 334 **4.2 – The sediment transport model**

335 The hydrodynamic model was coupled with a sediment transport model – MIKE 3 MT FM - valid for fine-grained and  
336 cohesive sediment (diameter smaller than 63  $\mu\text{m}$ , Lisi et al., 2017). This is the main type of sediment in the port of  
337 Genoa and is particularly relevant in terms of erosion, transport and further deposition, as its small particle dimension  
338 and light weight rapidly lead to its resuspension and advection around the basin.

339 The equations of the mud transport model are based on the advection and dispersion (AD) of the sediment concentration  
340 along the water column and are detailed in APPENDIX A2. The AD equation is solved using an explicit, third order  
341 finite difference scheme called ULTIMATE (Leonard, 1991).

342 The model consists of two areas: a water and a seabed environment. The seabed is represented through a multi-bed  
343 layer and multi-fraction approach in which the layers can exchange mass and only the top level is active, thus making it  
344 available for erosion. The different layers are defined by the proportions of sediment in their composition, the degree of  
345 consolidation of the sediment within each layer, and the thickness of the single layer. The sediment proportions are  
346 described through their associated physical characteristics, and are eroded and deposited proportionally to their  
347 concentration both in the bed texture and along the water column. Flocculation processes occur in the water  
348 environment of the model when a certain concentration threshold is exceeded (here assumed to be equal to 0.01  $\text{gl}^{-1}$ ),  
349 while at a threshold of 10  $\text{gl}^{-1}$  settling is hindered, according to the definition of Winterwerp and Kesteren (2004). The  
350 deposition of the sediment is based on a Teeter (1996) profile and the threshold for deposition used was 0.07  $\text{Nm}^{-2}$ . The  
351 sediment grain diameter is defined through the associated settling velocity, based on Stokes' law. In the interface  
352 between the water and the bottom the sediment may be eroded, as proposed by Partheniades (1965) for consolidated

353 sediment or by Parchure and Metha (1985) for soft or unconsolidated sediment. In both cases the sediment is eroded  
354 and injected into the water column when the shear stress resulting from the current, the wave action or a combination of  
355 both exceeds a certain critical value. We do not consider waves as our focus is inside the port.

356 The specific equations and parameterizations referred to in the sediment model are summarized in APPENDIX A2.

357

#### 358 4.2.1 - Sediment characteristics

359 Three sediment surveys were conducted between June 2009 and July 2010. Table 2 Table 2 presents the results of the  
360 surveys in terms of percentage and class of sediment per survey (last and central column, respectively). Given the  
361 nature of our study, our focus is on mud and fine sand, and thus grains coarser than 2 mm were not considered.

362 **Table 2 - Sediment size data inside the port (see station identified with the red dot of Figure 2). Three different**  
363 **surveys were carried out between June 2009 and July 2010**

Date of survey	Sediment Size	%
2009-06-15 16:00:00	$\emptyset < 63 \mu\text{m}$	82.4
2009-06-15 16:00:00	$63\mu\text{m} < \emptyset < 2\text{mm}$	16.2
2009-06-15 16:00:00	$\emptyset > 2 \text{ mm}$	1.4
2009-07-15 16:00:00	$\emptyset < 63 \mu\text{m}$	89.2
2009-07-15 16:00:00	$63\mu\text{m} < \emptyset < 2\text{mm}$	9.1
2009-07-15 16:00:00	$\emptyset > 2 \text{ mm}$	1.7
2010-07-28 09:00:00	$\emptyset < 63 \mu\text{m}$	78.2
2010-07-28 09:00:00	$63\mu\text{m} < \emptyset < 2\text{mm}$	17.7

364

365 We assumed that the proportions of the samples with  $\emptyset < 63 \mu\text{m}$  were composed of two grain sizes with diameters of 30  
366  $\mu\text{m}$  and 50  $\mu\text{m}$ , respectively, while for the observed components with diameters in the range of  $63\mu\text{m}$  to 2 mm we  
367 assumed 100  $\mu\text{m}$  to be representative.

368 The degree of consolidation of the seabed is both time- and depth-dependent. The upper layer, which mostly contributes  
369 to the flux of re-suspended sediments into the water column, is composed of freshly deposited sediment as it is subject  
370 to continuous reworking. The lower layers are more consolidated, and the degree of consolidation increases by depth.

371 This vertical gradient in seabed properties is enhanced in a port environment as the upper layers are continuously  
372 influenced by the propeller induced jets several times per day, hence a multilayer modelling of the seabed is  
373 appropriate. Teisson (1992) and Sandford and Maa (2001) also took this approach. A single layer bed representation  
374 would imply an overestimation of the bed's erodibility (soft mud, thus easily reworked), resulting in unrealistic further  
375 overestimations of sediment erosion and concentration along the water column. Thus, a multilayer representation of the  
376 seabed is required to account for the transition from unconsolidated to consolidated material. Amorim et al. (2010) used  
377 a two-layer approach to model the seabed with MIKE software, simulating the sediment transport in the navigation



378 channel of the Port of Santos. However, as they suggested, a two-layer representation of the seabed may produce an  
 379 unrealistically abrupt transition between erodible and hard bed layers, so to consider a gradual transition from freshly  
 380 deposited to consolidated material, three bed layers were defined here, representing the freshly deposited, slightly  
 381 consolidated and fully consolidated sediments. The percentage of the fine particles in the sediment texture was assumed  
 382 to decrease proportionally to the depth of the layers. Thus, the first layer contained 80% of fine grains (50% of grains of  
 383  $\Phi=30 \mu\text{m}$  and 30% of  $\Phi=50 \mu\text{m}$ ) and 20% of coarse ( $\Phi=100\mu\text{m}$ ), while the third layer contained 50% of coarse  
 384 ( $\Phi=100\mu\text{m}$ ) and 50% of fine (20% of grains of  $\Phi=30 \mu\text{m}$  and 30% of  $\Phi=50 \mu\text{m}$ ). In the mid layer, an even distribution  
 385 was assumed among the three. The thicknesses of the three layers are 0.5 mm, 1 mm and 50 mm at the beginning of each  
 386 scenario. The first layer is composed of very soft mud as it is the result of the newly deposited and finer mud. The other  
 387 two layers are more consolidated and thicker, as they are less easily eroded and are shielded by the upper layers. The  
 388 different layers and fractions of sediment that characterise the bottom enabled us to represent the port bed in a complex  
 389 and comprehensive way, and include the various degrees of consolidation of the layers and the resulting responses to  
 390 shear stress.

391 The main characteristics of the layers and sediment proportions implemented in the sediment transport model are  
 392 presented in Table 3 Table 3.

393 Finally, sediment input may also potentially come from six minor streams that flow into the port area. These have very  
 394 modest basins of approximately 1 km<sup>2</sup> on average, and have been ceiling-covered for many years, so they now act more  
 395 as sewage collectors than natural streams. Their contribution to the sedimentary dynamics of the port of Genoa has been  
 396 estimated and the annual sediment supply to the port basin from each stream evaluated, based on the method proposed  
 397 by Ciccacci et al. (1989). The estimated sediment contribution was only a few hundreds of cubic meters per year in the  
 398 worst case, which corresponds to a contribution to the wet basins of a few millimetres of annual accumulated sediment  
 399 from the surrounding river inlet. This level of solid matter has not been considered in the model as the erosional and  
 400 depositional processes induced by the propeller activity are higher by one or two orders of magnitude.

401

402 **Table 3 – Summary of sediment characteristics as implemented in the mud transport model**

<b>Parameter</b>	<b>Layer 1</b>	<b>Layer 2</b>	<b>Layer 3</b>
Layer thickness (mm)	0.5	1	50
Type of Mud	Soft	hard	hard
Dry density of bed layer (kgm <sup>-3</sup> )	180	300	450
<b>Parameter</b>	<b>Fraction 1</b>	<b>Fraction 2</b>	<b>Fraction 3</b>
$\Phi$ ( $\mu\text{m}$ )	30	50	100
% of fraction in layer 1, 2, 3	50, 33, 20	30, 33, 30	20, 33, 50
$W_s$ (mms <sup>-1</sup> )	0.7	2.2	8.8
$\tau_{ce}$ (Pa)	0.15	0.25	0.5

$\tau_{cd}$ (Pa)	0.07	0.07	0.07
$C_{floc}$ (g l <sup>-1</sup> )	0.01	0.01	0.01
$C_{hind}$ (g l <sup>-1</sup> )	10	10	10
$\rho_s$ (kg m <sup>-3</sup> )	2650	2650	2650

403

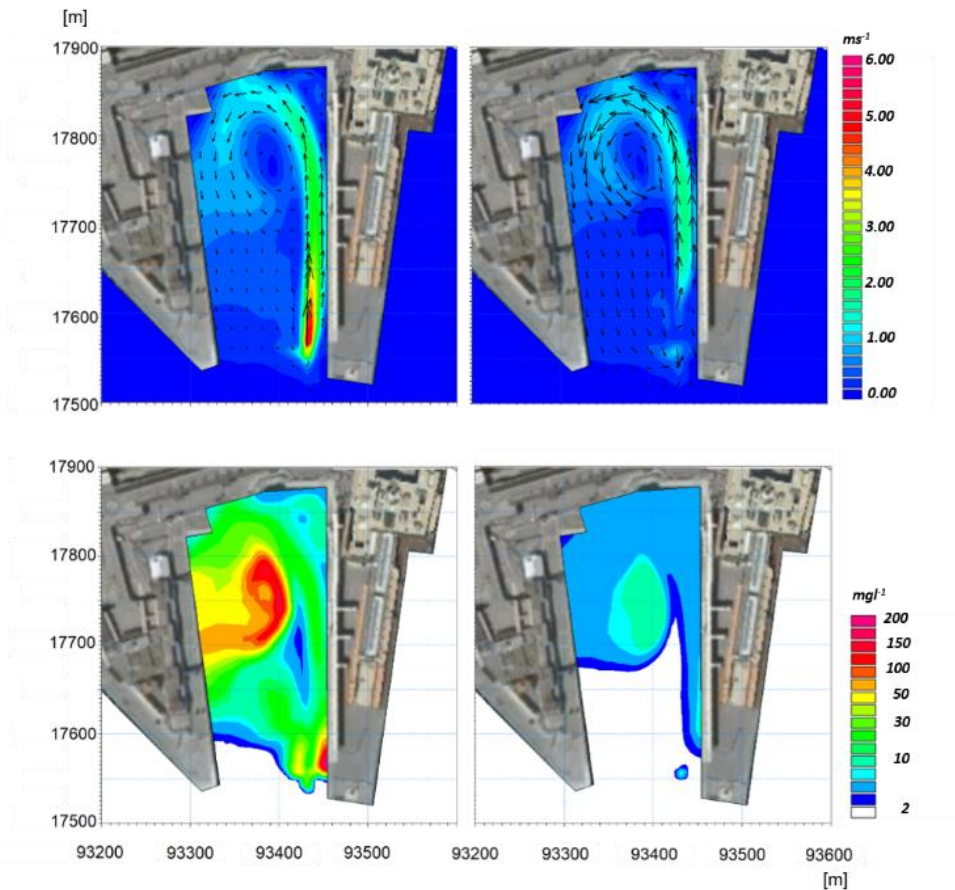
404

## 405 5 — Results and discussion

406 The main results of the hydrodynamic and sediment transport model are presented in this section. Due to the large  
407 number of simulations carried out, only those regarding two docks are shown. However, the current and sediment  
408 concentration results corresponding to the other simulations are qualitatively similar. We focus on the simulations of  
409 docks 1012 and T7. Dock 1012 is particularly important as it hosts the largest passenger vessels operating in the port,  
410 while dock T7 has a high frequency of passages.

411 Figure 7 shows the propeller-generated current in the bottom layer and at the depth of the propeller's axis (upper right  
412 and left panels, respectively) and the resulting suspended sediment concentration in the same layers (corresponding  
413 lower panels) during the departure of a cruise vessel from dock 1012. The characteristics of a vessel representative of  
414 the traffic in the dock are given in Table 1. When departing, the engine operates close to full power, which we  
415 assume results in a rotation rate of two rounds per second (rps) for the propeller. This induces a maximum velocity at  
416 the depth of the propeller axis close to 9 ms<sup>-1</sup>, which is damped to approximately 2 ms<sup>-1</sup> on the bottom of the berthing  
417 basin along the vessel's route. This intense jet is deflected to the left due to the head wall of the berthing basin, which  
418 constrains the flow and induces a cyclonic eddy that is well developed along the whole water column. The cone-like  
419 envelope of the jet in the vertical plane, as illustrated in the theoretical scheme of Figure 1 can be observed in  
420 the upper panels of Figure 7, which refer to the same example: the influence of the propeller on the bottom occurs  
421 several tens of meters behind the propeller's position, and the velocity at the bottom is much reduced. The induced eddy  
422 in the wet basin acts as a trap for the eroded sediment, which enters the cyclonic gyre (or anti-cyclonic in the case of  
423 departure from the opposite dock) and tends to deposit in the middle of the basin, where the fluxes progressively  
424 decrease. The position of the eye of the cyclone evolves parallel to the docks' longitudinal walls and induces the  
425 sediment trapped inside the gyre to sink along the longitudinal axis of the wet basin. Such dynamic occurs similarly for  
426 all the horseshoe-shaped wet basins, inducing accumulation along the central portions. The re-suspended sediment may  
427 reach very high concentrations of up to several hundreds of mg l<sup>-1</sup> in the bottom layers, depending on the different  
428 specific characteristics of the sediment texture (such as grain size, level of consolidation and availability to erosion) and  
429 of the vessel (such as dimensions of the propellers, rotation rate and draught).

430 Various hydro and sediment dynamics occur during the inbound phase of vessels manoeuvring inside the port. Most of  
431 the manoeuvring operations (i.e., when vessels rotate within a turning basin and proceed backwards to the docks) occur  
432 in the turning basins denoted by the dashed circles *a* and *b* in Figure 2Figure 2. The engines operate at high power  
433 when starting the manoeuvre, to allow for the rotation of the ship. The vessel's longitudinal axis then rapidly changes  
434 direction (from tens of seconds up to a few minutes) and can span wide angles, depending on the specific manoeuvre.  
435 The propeller induced jet follows the same rotation along the horizontal plane, resulting in a fan-like distributed set of  
436 directions for the associated currents. Such operations are realistically represented by the model, as shown in Figure 8,  
437 which refers to the berthing of the vessel representative of dock T7. The currents shown in the figure are those  
438 associated with the propeller's axis during four different moments of the turning manoeuvre. Each panel refers to  
439 successive time intervals of approximately 100 seconds. These successive instants are presented in the order of up-left,  
440 up-right, down-left and down-right. In the lower-right panel the propeller has already changed rotation direction and the  
441 vessel is now proceeding backwards. The induced current jet is thus heading towards the centre of the port and pushing  
442 the sediment towards this area. The simultaneous seabed activity is shown in Figure 9Figure 9. Although the jet  
443 induced currents are very much weaker at the seabed than those at the depth of the propeller's axis, they are still  
444 significant and may reach intensities of up to  $1 \text{ ms}^{-1}$ , depending on the local bathymetry.  
445

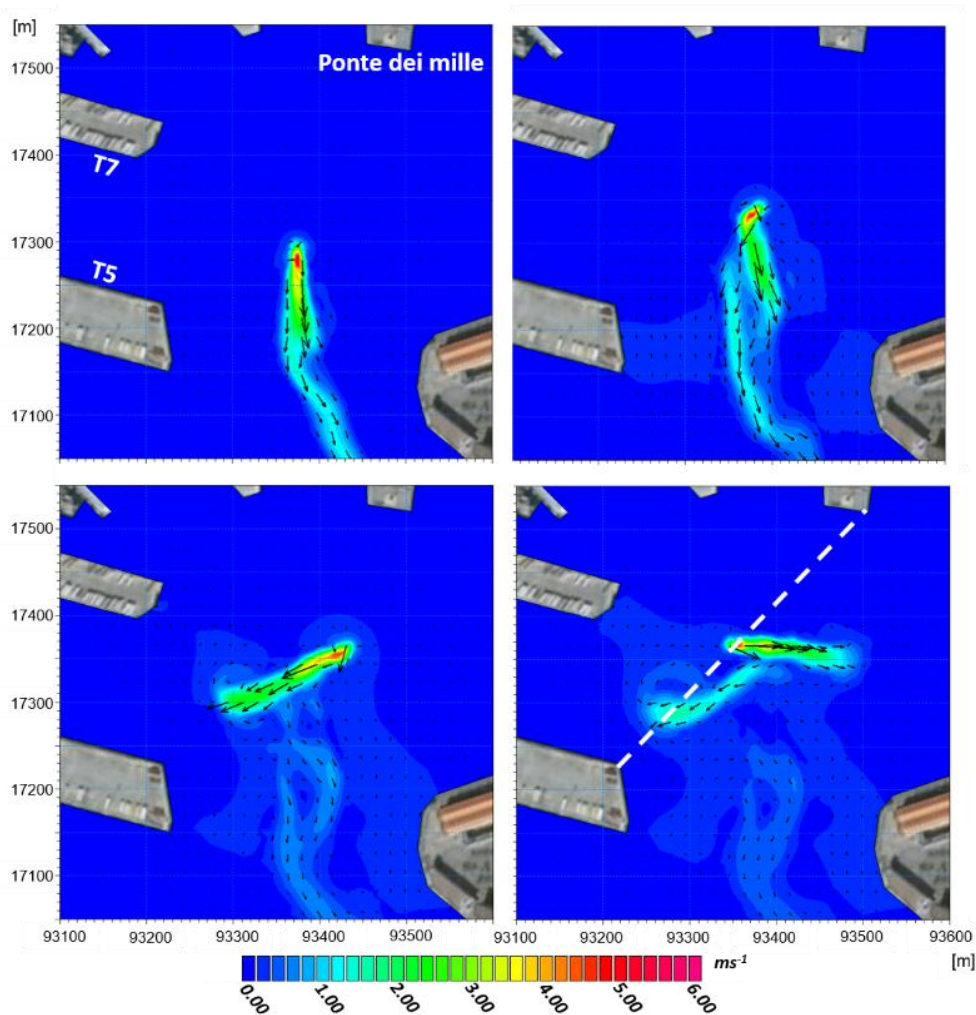


446

447 **Figure 7 – Results of the numerical models. Upper panels: current intensity and direction in the bottom layer**  
 448 **(right) and in the layer corresponding to the axis propeller. Lower panels: resulting suspended sediment**  
 449 **concentration (SSC,  $mg l^{-1}$ ) in the same layers as the upper panels. The images refer to the undocking of the**  
 450 **cruise vessel representative of dock 1012.**

451 The current distribution at the seabed is much more chaotic than at the propeller's axis depth. This area of the port  
 452 corresponds to the natural pit (which reaches approximately 22 meters below the surface in the deeper part) in which the  
 453 material dredged from the accumulation areas is often dumped during the sea bottom maintenance activities. The  
 454 dashed line shown in the lower-right panels of Figure 8 and Figure 9 Figure 9 refers to the transect presented in  
 455 **Errore. L'origine riferimento non è stata trovata.Errore. L'origine riferimento non è stata trovata.** in the same  
 456 instant (i.e. when the vessel has ended the manoeuvre in the circle *b* and is approaching dock T7 backwards).

457



458

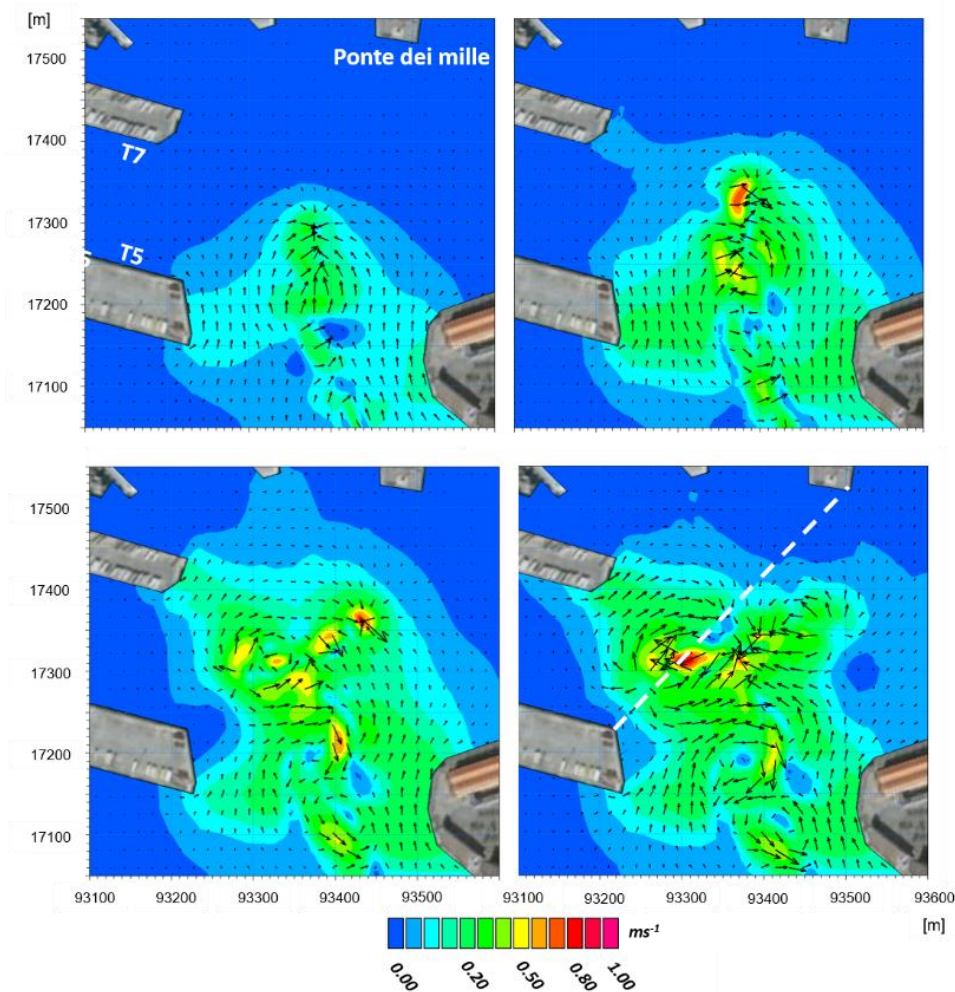
459 **Figure 8 – Results of the hydrodynamic model at the depth of the propeller’s axis. Each panel refers to a time**  
 460 **interval of approximately 100 seconds from the previous one. The temporal order of the panels is up-left, up-**  
 461 **right, down-left and down-right. The images refer to docking maneuvers of the Ro-Ro vessel representative of**  
 462 **dock T7**

463

464 A combined analysis of Figure 8, Figure 9Figure 9 and **Errore. L'origine riferimento non è stata trovata.Errore.**

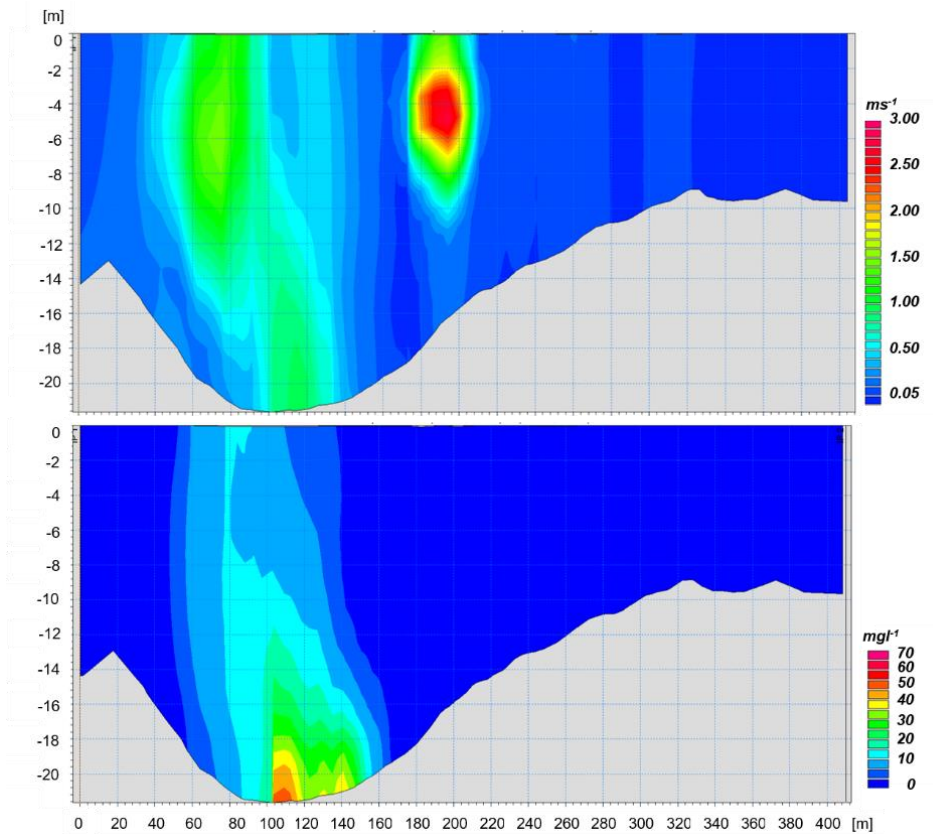
465 **L'origine riferimento non è stata trovata.** helps us understand the dynamics occurring in the turning basin *b* during  
 466 the manoeuvres when approaching docks T5, T6 and T7, and particularly the overall sediment dynamics of the entire  
 467 port, as these three docks account for approximately half of the entire passenger traffic. The propeller-induced velocities  
 468 at the bottom of the natural pit during turning manoeuvres are variable and may exceed  $1 \text{ ms}^{-1}$ , which is a significant  
 469 current intensity that can entrain and move a large amount of sediment. The resulting re-suspended sediment  
 470 concentration may reach values exceeding  $50\text{-}60 \text{ mg l}^{-1}$ , as shown in the lower panel of **Errore. L'origine riferimento**  
 471 **non è stata trovata.Errore. L'origine riferimento non è stata trovata.**.. Once re-suspended from the pit, the sediment

472 is advected by the jet-induced complex field of currents of Figure 8 and Figure 9. This area is typically  
 473 refilled with freshly dredged material resulting from the seabed maintenance activities, and thus the propeller's induced  
 474 currents on the bottom have an enhanced erosion effect on the unconsolidated material and can rapidly nullify the  
 475 benefit of the dredging operations. Thus, the results of the simulations suggest avoiding the use of the natural pit as a  
 476 dumping area for the resulting material, and confirm that integrated modelling can be an effective tool for simulating  
 477 the processes and mechanisms related to sediment transport, and for the optimized planning of maintenance activities.



478  
 479 **Figure 9 – Results of the hydrodynamic model in the bottom layer. Each panel refers to a time interval of**  
 480 **approximately 100 seconds from the previous one. The temporal order of the panels is up-left, up-right, down-**  
 481 **left and down-right. The images refer to docking maneuvers of the Ro-Ro vessel representative of dock T7**

482  
 483

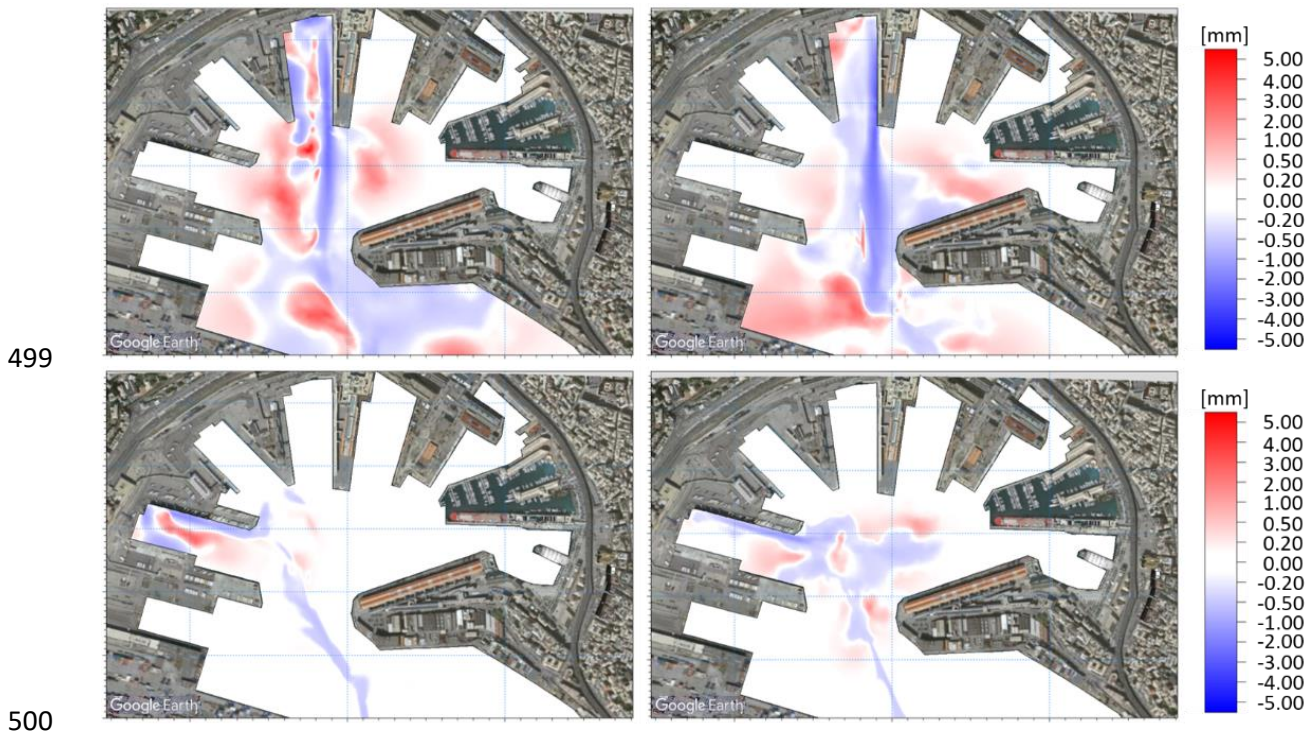


485

486 **Figure 10 - Velocity intensity in  $ms^{-1}$  (upper panel) and sediment concentration in  $mg l^{-1}$  (lower panel) along the**  
 487 **transect from the head of *Ponte Assereto* to the head of *Ponte dei Mille***

488

489 The impact on the bed thickness of the naval traffic is illustrated in Figure 11, which presents the erosion  
 490 and deposition maps resulting from the simulations of one departure (left) and one arrival (right) of the representative  
 491 passenger vessels of docks 1012 (up) and T7 (down). The blue color represents areas of erosion, while the red  
 492 represents the accumulation of the sediment after an interval of time long enough for the re-suspended sediment to  
 493 completely settle. The left panels of the figure show that during the vessel's departure a considerable amount of material  
 494 tends to be eroded from the bases of the docks and settles in the center of the mooring basins. This mechanism is clearly  
 495 related to the vessel's departure (left panels) rather than its arrival (right panels). The erosion underneath the vessel's  
 496 keel along the ship's trajectory is evident, both during departure and arrival, thus supporting previous experimental  
 497 findings (Castells et al., 2018). The order of magnitude of erosion and deposition of a single vessel's passage is of a few  
 498 millimeters in the areas most influenced by the vessel's activity.



501 **Figure 11 – Erosion and deposition maps resulting from one departure (left) and one arrival (right) of the**  
 502 **representative passenger vessels of docks 1012 (up) and T7 (down)**

503 Such impact can become a real threat to the continuity of operations in large and busy ports such as Genoa over medium  
 504 to long timescales. The few millimeters of accumulation and erosion can become several tens of centimeters after a few  
 505 thousand annual passages. For the sake of completeness, the results of the impact on the bed thickness due to the  
 506 activity of the other vessels not shown here are presented in APPENDIX A3.

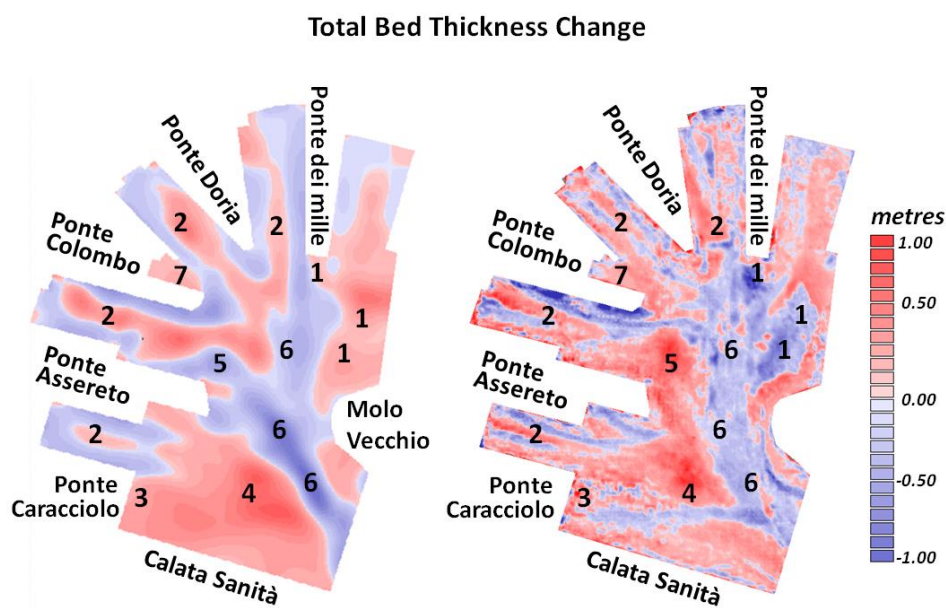
507 Based on the traffic analysis of Table 1 we projected each single naval passage to a one-year duration and  
 508 superimposed the effects of erosion and deposition of vessels that are representative of all of the passenger docks. We  
 509 were thus able to reconstruct the annual port seabed evolution for the year of 2017. The effects of the single passages  
 510 were weighted by the specific occurrences of that year, thus obtaining 24 maps (one for each docking and one for each  
 511 undocking), and the results were integrated to obtain a final map.

512 As the trajectories for reaching a dock (or departing from it) vary slightly from passage to passage, a Bartlett spatial  
 513 filter was applied to the integrated results using the values of 4, 2 and 1 as weights. Figure 12 presents the  
 514 results of this analysis. In the left panel the results from the modeling system in terms of annual erosion (blue) and  
 515 accumulation (red) are shown, while in the right panel the observed seabed evolution is shown. The observed map was  
 516 reconstructed using the outcomes of two bathymetric surveys carried out in the periods of May-June 2017 and March-  
 517 June 2018. The difference in the bathymetries of the two surveys resulted in the evolution of the seabed during the



518 approximate one-year period, except for dredging operations. We indicated the areas where the most significant  
519 dynamics took place on the maps using numbers.

520 The area between the heads of *Ponte dei Mille* and of *Molo Vecchio*, identified as 1, was dredged during the period  
521 October-December 2017, and approximately 15.000 m<sup>3</sup> of solid material was removed and dumped into the natural pit  
522 of the port, as indicated by the number 5. Thus, what appears to be at first sight an area of erosion due to vessel traffic -  
523 area 1 in the right panel of Figure 12Figure 12 - is actually an area of accumulation, which is confirmed by the fact  
524 that dredging operations were conducted. Similarly, the accumulation observed in area 5 (right panel of Figure  
525 12Figure 12) is not the result of the induced action of the propellers, but of the accumulation of the sediment dumped  
526 after the maintenance dredging operations. The model results are in total agreement with these dynamics. As discussed  
527 above, the material re-suspended during vessels' maneuvers is likely pushed towards area 1 during the phase of the  
528 backward advancing of the vessels when approaching the docks. Conversely, area 5 is partially an area of erosion, as  
529 evidenced by the model. The freshly deposited material during dredging operations is thus rapidly re-suspended.



530

531 **Figure 12 – Annual erosion and deposition map reconstructed on the basis of the hydrodynamic and sediment**  
532 **transport simulations for the year 2017**

533 Area 1 accounts for approximately 30-40 cm of accumulated material per year, with local maxima of up to 50 cm.  
534 Similar values were estimated through years of managing experience by the personnel of Stazioni Marittime S.p.A  
535 (personal communication).

536 The central portions of the wet basins marked with number 2 in Figure 12Figure 12 are areas of deposition, mainly  
537 due to the phase of departure of the ships. Again, the model can well reproduce both the accumulation along the central

538 parts of the basins, where it may reach 20 cm per year or even more, and the erosion along the walls of the docks. Here,  
539 the propellers' erosive action may result in stability problems for the docks, particularly along the walls of dock 1012,  
540 where the biggest cruise vessels operate.

541 The erosion underneath the vessels' typical routes (i.e., from the entrance to approximately the center of the port) is also  
542 well represented by the model, and is identified in the figure with the number 6. The model and the observations also  
543 exhibit good agreement in the deposition area (number 7), where a local gyre forms and entraps the suspended  
544 sediment. Finally, areas 3 and 4 are also subject to deposition, and qualitative agreement between the model and the  
545 various bathymetric surveys is evident from Figure 12. The erosive print observed in the survey under these  
546 areas is most likely due to activities related to cargo vessels approaching and departing from dock *Calata Sanità*. These  
547 vessels were not the focus of our study, and *Calata Sanità* only operates container ships, and thus the model does not  
548 include the naval traffic here.

549 In general, the observed and the modeled annual evolution of the port seabed show very good agreement, which  
550 confirms the reliability and robustness of the hydrodynamic and sediment transport model and demonstrates the  
551 potential importance of an integrated modeling approach in optimizing the management of port activities.

552 The assumption of unvarying initial bathymetry conditions in the different scenarios deserves some additional  
553 consideration, as it undoubtedly introduces some inaccuracy into the results. This approach does not consider the real  
554 order of vessels' passages or the impact that the evolving seabed has on the hydrodynamics and sediment transport  
555 simulations. In particular, the variable clearance distance between the propeller's tip and the seabed due to the evolving  
556 erosion/deposition processes is not considered, although this will increase the differences over time. However, the  
557 complexity of the system requires the introduction of several approximations, such as the dimension and rotation rates  
558 of the propellers, the typology and distribution of the sediment, the layering of the sea bed, the shear stress for erosion  
559 and deposition, or the constant initial bathymetry. A solution for the bathymetry issue could be to implement the system  
560 in operational mode, and thus continually updating the initial bottom boundary conditions through the simulation  
561 iterations. However, this was not realistic in terms of computational effort, and was beyond the scope of the study,  
562 which was to identify areas of erosion and deposition in the port and to evaluate the order of magnitude of the  
563 corresponding evolution rates to support the port management. Nevertheless, if we consider the most significant  
564 variation of the seabed and the typical propeller induced bottom velocities, which are in the order of 50 cm (Figure 12)  
565 and  $1-2 \text{ ms}^{-1}$  (Figures 7, 9 and 10), respectively, the resulting bottom shear stresses are in the order of  $2-4 \text{ Nm}^{-2}$ . Such  
566 values are orders of magnitude larger than the typical critical shear stress for the deposition-erosion of freshly deposited  
567 fine sediments (in the order of  $0.07-0.15 \text{ Nm}^{-2}$ , respectively), suggesting that variations in the bottom shear stresses due  
568 to a change in the clearance distance of the propeller's tip of an order of 50 cm (a conservative estimate), would not

569 have a significant impact on the mobility of the sediments. Consequently, such differences would not imply substantial  
570 variations in the erosional and depositional processes and patterns.

## 571 **5 – Summary and Conclusions**

572 The impact of naval traffic on the seabed of the passenger port of Genoa was investigated through numerical modeling.  
573 The combination of a very high resolution, non-hydrostatic, circulation model (MIKE 3 HD FM) with a sediment  
574 transport model (MIKE 3 MT FM), based on unstructured grids on the horizontal and on sigma levels on the vertical,  
575 enabled us to reconstruct the annual evolution of the port seabed. The final results of the modeling, in terms of maps of  
576 erosion and deposition inside the basin, were qualitatively supported by observational evidence. Our approach was to  
577 simulate only one arrival and one departure from each dock of the port and to analyze the impact of a single naval  
578 passage on the seabed in terms of sediment concentration, motion and distribution.

579 From the traffic analysis in the port for a typical year (2017), we could obtain the detailed situation of the number of  
580 arrivals and departures for each dock as a starting point for the study. By superimposing the effects of single vessels  
581 weighted for the annual number of passages of the most representative vessel operating on each dock, an annual map of  
582 erosion/deposition was reconstructed and validated on a semi-quantitative basis by comparison with various  
583 bathymetric surveys for the same period.

584 In general, the simulations showed that the velocity intensities on the bottom induced by propeller-generated jets can  
585 reach almost  $2 \text{ ms}^{-1}$ , and mainly depend on the dimensions of the propellers, the rotation rate and the distance between  
586 the propeller and the bottom. Such velocities may reach up to  $8\text{-}9 \text{ ms}^{-1}$  at the propeller's axis depth, and penetrate  
587 horizontally through the water for long distances, up to at least 40-50 times the propeller's diameter. The bed shear  
588 stresses induced by these velocities, and the propeller jet induced entrainment, mobilize and re-suspend large amounts  
589 of the fine and less compacted sediments present inside the port. Fine proportions with lower fall velocities tend to  
590 remain in suspension for longer periods of time, resulting in the creation of sediment plumes.

591 Our findings showed how significant these deposition rates can be in a densely operated port, reaching values of several  
592 tens of centimeters per year in specific areas.

593 Our approach enabled us to minimize the computational time and also decompose the overall complex view of sediment  
594 transport of the entire port into several simpler views. Consequently, we were able to analyze the specific hydro and  
595 sediment dynamics for each dock and vessel, and to identify specific routes responsible for particularly serious erosion  
596 and accumulation, as historically reported by the managing authorities of the port operations and traffic. The range of  
597 current intensities induced by the propeller action was identified along the water column, and this can be further used as  
598 a sound and scientifically based benchmark value for potential defensive actions on the seabed and port structures, to  
599 guarantee the ongoing full operability of the port.

600 The most significant mechanisms for the port's hydro and sediment dynamics that occur during vessel passages were  
601 identified and the subsequent analysis identified how and why specific areas are subject to erosion and other areas are  
602 subject to deposition, and the extent of these mechanisms. In particular, the mechanism of ongoing erosion along the  
603 docks walls and of deposition along the central portions of the mooring basins were identified and explained, along with  
604 the ongoing deposition process in the area between the heads of *Ponte dei Mille* and *Molo Vecchio*. Identifying and  
605 reproducing this process for the port managers was particularly important as it occurs at a very significant rate of up to  
606 40-50 cm per year in some areas. Finally, the natural hole located off the heads of *Ponte Colombo* and *Ponte Assereto*  
607 was identified through the model as an area of erosion, although at significant depth. This is mainly due to the turning  
608 maneuvers carried out by vessels in this area, and partially corresponds to one of the turning basins of the port and  
609 involves approximately 50% of its entire traffic (docks T5, T6 and T7). This location has historically been used as a  
610 dumping site for the material resulting from seabed maintenance dredging, but our study showed how unfit this area is  
611 for such purpose, as the freshly deposited sediment is soon re-suspended by the intense currents induced by the vessels  
612 turning operations.

613 The importance of this study is not only to confirm how an integrated high resolution modeling can reproduce the most  
614 significant and complex mechanisms of hydrodynamics and sediment transport occurring inside ports, which was  
615 successfully achieved, but it also suggests that it can be used as a tool for optimizing port management. It could be  
616 applied to regulating the naval traffic in ports and thus identifying the most suitable schedule and routing in terms of  
617 sediment concentrations, bottom velocities, erosion, accumulation and vessel drafts. It could also be used to identify the  
618 largest vessels that can potentially operate in the docks when planning future commercial traffic, or to study the impact  
619 of increased port traffic on the seabed and on the port's structures. Finally, in recurring dredging operations, most busy  
620 ports must regularly face sediment accumulation problems, and our tool can therefore inform awareness planning of  
621 such activities so the authorities are fully prepared.

622 Daily fully-operational implementations of similar integrated systems can also be set up, as the daily schedule of the  
623 port is known. This would enable the continuous monitoring of the evolution of the seabed and allow authorities to be  
624 constantly and fully aware of the potential criticalities they face.

625 Future research following on from this study should also consider the effect of the Bernoulli wake in combination with  
626 the propeller's induced jets on sediment resuspension, advection and dispersion. This mechanism was not considered in  
627 the present version of the system. The current intensities caused by vessels' generated waves during and after their  
628 passages will be smaller than those induced by propellers along their axes, but they tend to penetrate along the water  
629 column and reach the bottom, thus carrying a significant amount of energy, and possibly re-suspending a substantial

630 amount of solid material (Rapaglia et al., 2011), which is likely to enhance vertical mixing and may induce the sediment  
 631 to be suspended for longer periods and at higher depths.

632

633 **APPENDIX A1 – Hydrodynamic model governing equations**

634 MIKE 3 Flow Model FM is based on the Navier-Stokes equations for an incompressible fluid under the assumptions of  
 635 Boussinesq. The governing equations of the model are the equations of momentum (A1.1) and mass continuity (A1.2),  
 636 the equations of heat and salinity transport (A1.3 and A1.4, respectively) and the equation of state (A1.5) based on the  
 637 UNESCO formula of 1981 (UNESCO, 1981a). Considering a Cartesian coordinate system  $(x,y,z)$  we have:

638 
$$\frac{\partial u}{\partial x} + \frac{\partial v}{\partial y} + \frac{\partial w}{\partial z} = 0 \quad (\text{A1.1})$$

639

640 
$$\frac{\partial u}{\partial t} + \frac{\partial u^2}{\partial x} + \frac{\partial uv}{\partial y} + \frac{\partial wu}{\partial z} = fv - \frac{1}{\rho_0} \frac{\partial q}{\partial x} - g \frac{\partial \eta}{\partial x} - \frac{1}{\rho_0} \frac{\partial p_a}{\partial x} - \frac{g}{\rho_0} \int_z^\eta \frac{\partial \rho}{\partial x} dz + F_u + \frac{\partial}{\partial z} \left( \nu_t^v \frac{\partial u}{\partial z} \right) \quad (\text{A1.2.1})$$

641

642 
$$\frac{\partial v}{\partial t} + \frac{\partial v^2}{\partial y} + \frac{\partial uv}{\partial x} + \frac{\partial wv}{\partial z} = fu - \frac{1}{\rho_0} \frac{\partial q}{\partial y} - g \frac{\partial \eta}{\partial y} - \frac{1}{\rho_0} \frac{\partial p_a}{\partial y} - \frac{g}{\rho_0} \int_z^\eta \frac{\partial \rho}{\partial y} dz + F_v + \frac{\partial}{\partial z} \left( \nu_t^v \frac{\partial v}{\partial z} \right) \quad (\text{A1.2.2})$$

643

644 
$$\frac{\partial w}{\partial t} + \frac{\partial w^2}{\partial z} + \frac{\partial uw}{\partial x} + \frac{\partial wv}{\partial y} = -\frac{1}{\rho_0} \frac{\partial q}{\partial z} + F_w + \frac{\partial}{\partial z} \left( \nu_t^v \frac{\partial w}{\partial z} \right) \quad (\text{A1.2.3})$$

645

646 
$$\frac{\partial T}{\partial t} + \frac{\partial uT}{\partial x} + \frac{\partial vT}{\partial y} + \frac{\partial wT}{\partial z} = F_T + \frac{\partial}{\partial z} \left( D_{ts}^v \frac{\partial T}{\partial z} \right) + \hat{H} \quad (\text{A1.3})$$

647

648 
$$\frac{\partial S}{\partial t} + \frac{\partial uS}{\partial x} + \frac{\partial vS}{\partial y} + \frac{\partial wS}{\partial z} = F_s + \frac{\partial}{\partial z} \left( D_{ts}^v \frac{\partial S}{\partial z} \right) \quad (\text{A1.4})$$

649

650 
$$\rho = \rho(S, T) \quad (\text{A1.5})$$

651 Since we used the barotropic density mode the only hydrodynamic equations used for the present work  
 652 are A1.1 and A1.2. The symbols used in the governing equations of the model are presented in Table 4

653 **Table 4 – Symbols used in the governing equations A1**

$x,y,z$	Cartesian coordinate system
$u,v,w$	components of the field of velocity [ $\text{ms}^{-1}$ ]
$g$	gravity acceleration [ $\text{ms}^{-2}$ ]
$\rho$	water density [ $\text{kgm}^{-3}$ ]
$\rho_0$	reference value for water density [ $\text{kgm}^{-3}$ ]
$q$	non-hydrostatic pressure [Pa]
$p_a$	atmospheric pressure at the sea surface [Pa]
$f$	Coriolis parameter (non-dimensional)

$\nu_t^v$	vertical eddy viscosity [ $\text{m}^2\text{s}^{-1}$ ]
$F_u, F_v, F_w$	horizontal diffusivity
$T$	temperature [ $^{\circ}\text{C}$ ]
$S$	Salinity [PSU]
$F_T, F_S$	Horizontal diffusion terms for $T$ and $S$
$D_{ts}^v$	vertical eddy diffusivity [ $\text{m}^2\text{s}^{-1}$ ]
$\hat{H}$	Source term due to heat exchange with the atmosphere

654

## 655 APPENDIX A2 – Mud transport model governing equations and parameterizations

656 The sediment transport module is based on the advection dispersion equation for a passive tracer in an incompressible  
657 fluid. The tracer is the concentration  $C$  of sediment along the water column. The field velocity used for advection is the  
658 one calculated through the hydrodynamic set of equations of Appendix A1. The symbols used in the set of equations A2  
659 are summarized in Table 5

$$660 \quad \frac{\partial C}{\partial t} + \frac{\partial}{\partial x}(uC) + \frac{\partial}{\partial y}(vC) + \frac{\partial}{\partial z}[(w + w_s)C] = \frac{\partial}{\partial z}\left(D_C^v \frac{\partial C}{\partial z}\right) + F_C \quad (\text{A2.1})$$

661 The vertical bottom boundary condition for sediment flux is expressed as:

$$662 \quad D_C^v \frac{\partial C}{\partial z} \Big|_{z=-H} - w_s C = S \quad (\text{A2.2})$$

663 and the sediment flux  $S$  at the bottom is calculated through the approach of Krone (1962) for deposition (Eq. A2.3),  
664 through that of Partheniades (1965) for erosion of consolidated sediment (Eq. A2.4) and through that of Parchure and  
665 Metha (1985) for erosion of soft or unconsolidated sediment (Eq. A2.5).

$$666 \quad S_d = w_s c_b p_d \quad (\text{A2.3})$$

667 where

$$668 \quad p_d = 1 - \frac{\tau_b}{\tau_{cd}} \quad \text{valid for } \tau_b < \tau_{cd} \quad (\text{A2.3.1})$$

$$669 \quad S_{ec} = E \left( \frac{\tau_b}{\tau_{ce}} - 1 \right)^n \quad \text{valid for } \tau_b \geq \tau_{ce} \text{ and hard bed} \quad (\text{A2.4})$$

$$670 \quad S_{es} = E \exp[\alpha(\tau_b - \tau_{ce})^{1/2}] \quad \text{valid for } \tau_b \geq \tau_{ce} \text{ and soft bed} \quad (\text{A2.5})$$

671 The settling velocity for sediment is calculated through the Stokes law (A2.6).

$$672 \quad w_s = \frac{gd^2}{18} \left( \frac{\rho_s}{\rho_w} - 1 \right) \quad (\text{A2.6})$$

673 **Table 5 – symbols used in the equations and parameterizations A2 of the sediment transport model**

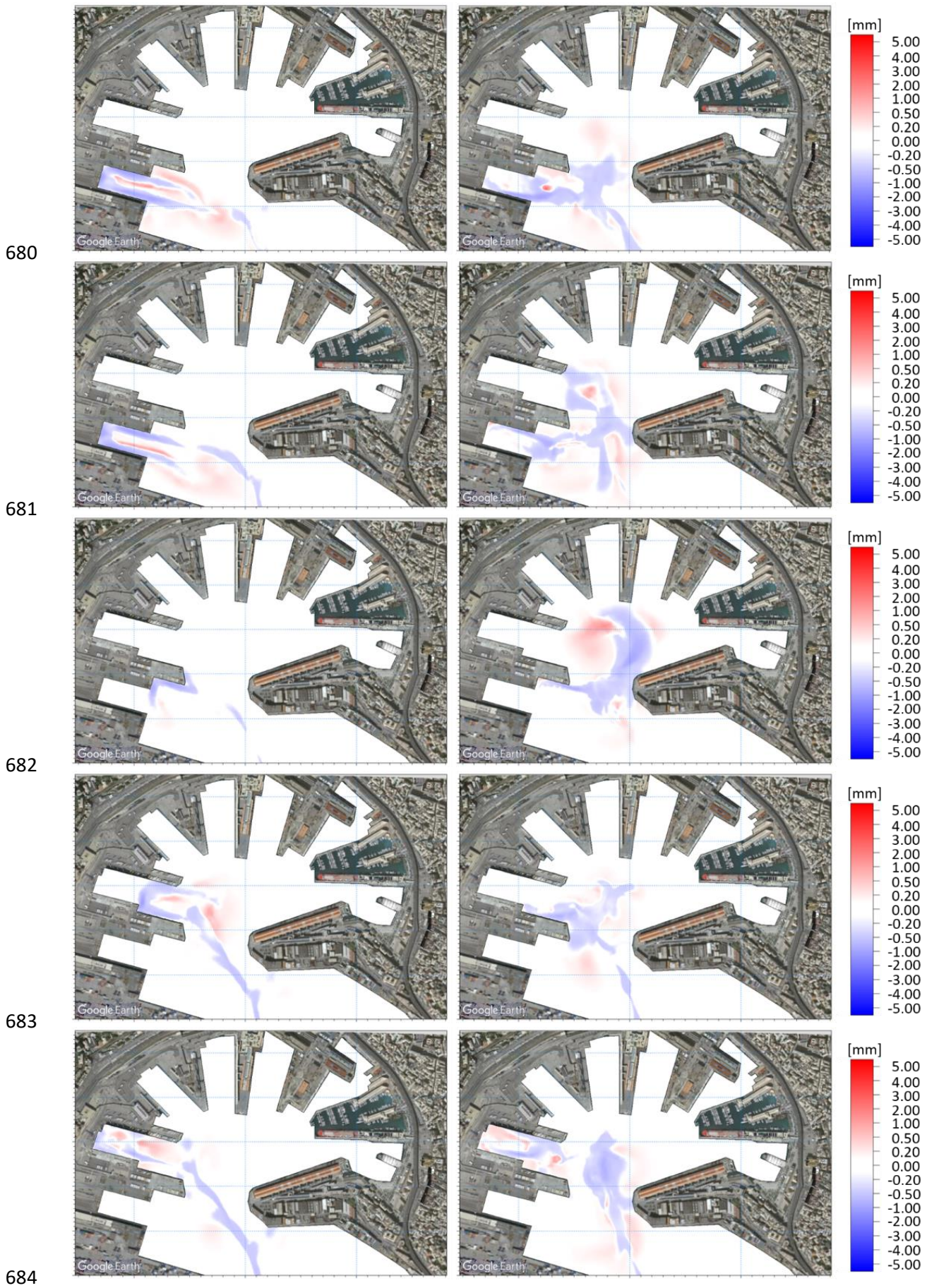
$x,y,z$	Cartesian coordinate system (same as Table 4)
$u,v,w$	components of the field of velocity (same as Table 4) [ $\text{ms}^{-1}$ ]
$C$	sediment concentration [ $\text{gmc}^{-1}$ ]
$C_b$	sediment concentration in the bottom layer [ $\text{gmc}^{-1}$ ]
$w_s$	settling velocity [ $\text{ms}^{-1}$ ]
$D_C^v$	vertical eddy diffusivity for $C$ (same as for $T$ and $S$ ) [ $\text{m}^2\text{s}^{-1}$ ]
$F_C$	horizontal diffusion terms for $C$
$H$	water depth [m]
$S_e$	bottom sediment flux for erosion [ $\text{kgm}^2\text{s}^{-1}$ ]
$S_d$	bottom sediment flux for deposition [ $\text{kgm}^2\text{s}^{-1}$ ]
$S_{e,s}$	bottom sediment flux for erosion of soft bed [ $\text{kgm}^2\text{s}^{-1}$ ]
$S_{e,c}$	bottom sediment flux for erosion of consolidated bed [ $\text{kgm}^2\text{s}^{-1}$ ]
$p_d$	probability of deposition for the sediment [non dimensional]
$\tau_b$	bottom shear stress [ $\text{Nm}^{-2}$ ]
$\tau_{bd}$	critical stress for deposition [ $\text{Nm}^{-2}$ ]
$\tau_{ce}$	critical stress for erosion [ $\text{Nm}^{-2}$ ]
$E$	bottom erodibility [ $\text{Nm}^{-2}$ ]
$\alpha$	empirical coefficient [ $\text{m}/\sqrt{N}$ ]
$n$	Power of erosion (empirical non-dimensional)
$d$	diameter of grains [m]
$\rho_s$	density of dried sediment [ $\text{kgm}^{-3}$ ]
$\rho_w$	density of water [ $\text{kgm}^{-3}$ ]
$g$	gravity acceleration [ $\text{ms}^{-2}$ ]

674

675

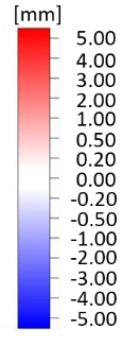
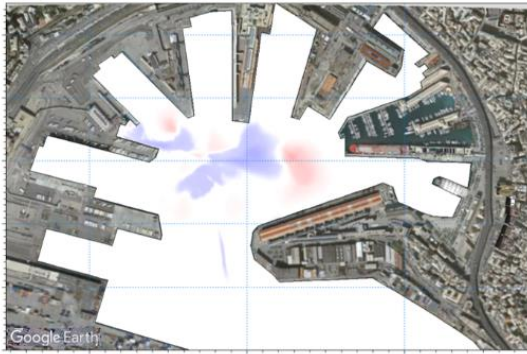
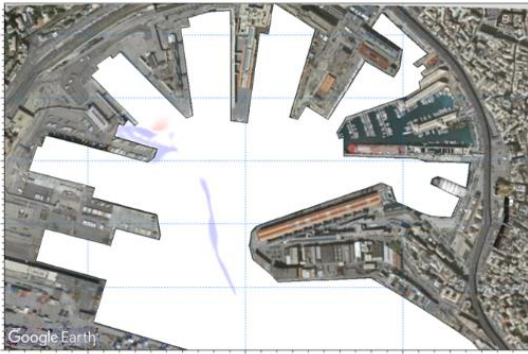
676 **APPENDIX A3 – Results of total bed change**

677 The following matrix of plots presents the results in terms of sediment erosion and accumulation for a single undocking  
 678 (left) and docking (right) respectively for the scenarios of docks T1, T2, T3, T5, T6, T9, T10, T11, DL, 1003, (top to  
 679 bottom).

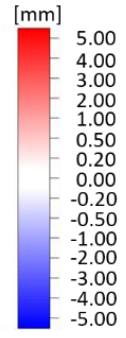
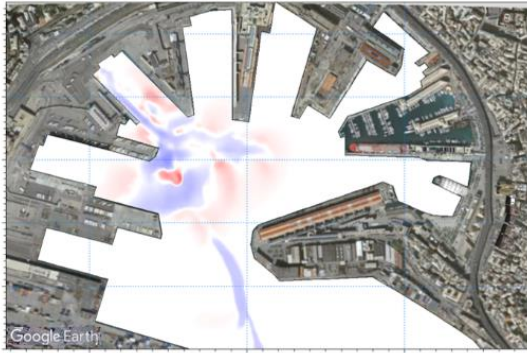
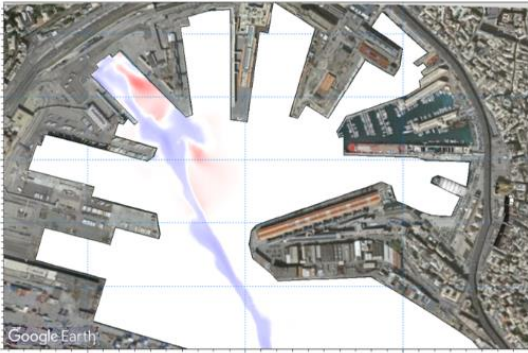




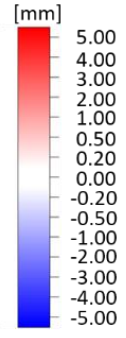
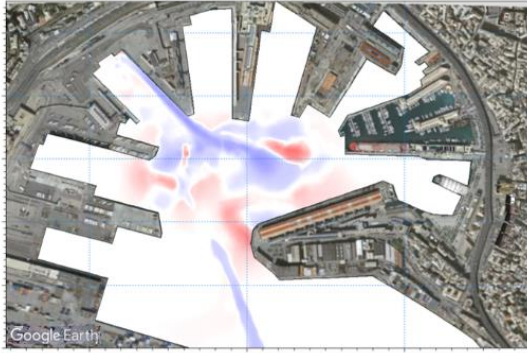
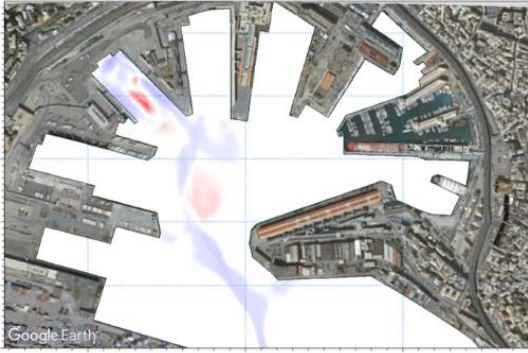
685



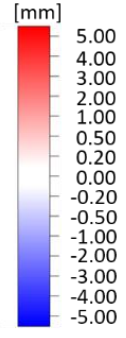
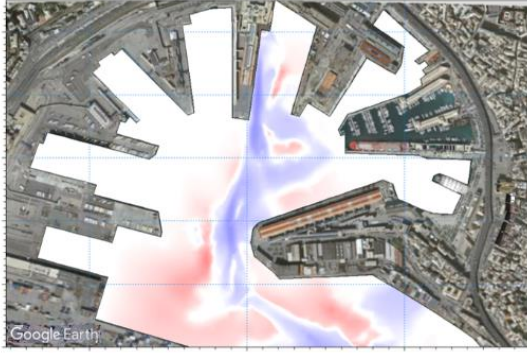
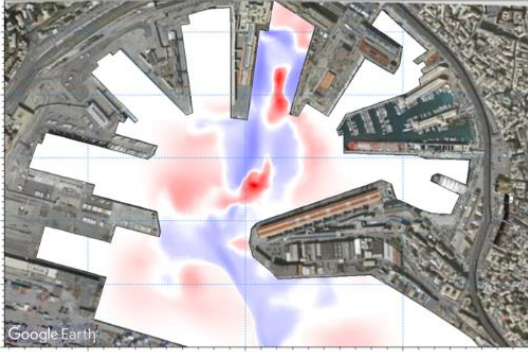
686



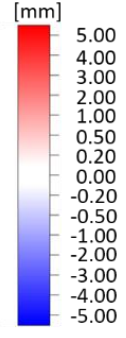
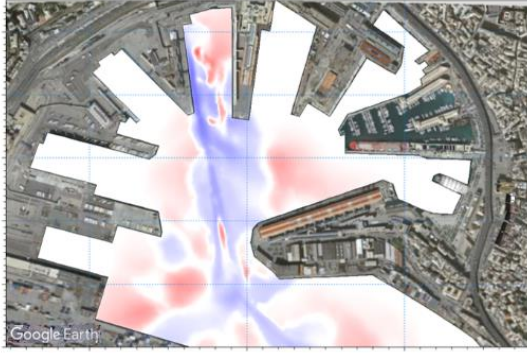
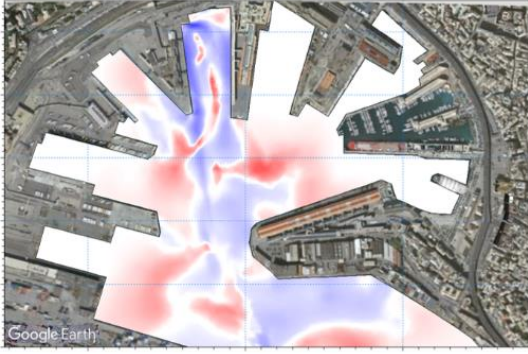
687



688



689



690

691 **Data Availability**

692 The modelling dataset including the simulations produced for the present study covers a volume wider than 2 TB. Such  
693 an amount of data raises an evident problem in order to make them available on data repositories. Consequently, the  
694 output of the simulations won't be directly available. However, the model set-up and all the files necessary for their  
695 reproduction will be made available in MIKE FM format upon request to the corresponding author.

696

697 **Team list**

698 Antonio Guarnieri (first and corresponding author), Sina Saremi (co-author), Andrea Pedroncini (co-author), Jakob H.  
699 Jensen (co-author), Silvia Torretta (co-author), Caterina Vincenzi (co-author), Marco Vaccari (co-author).

700

701 **Author contributions:**

702 Antonio Guarnieri implemented the numerical models and simulations, post-processed the raw output, analysed the  
703 results and wrote the manuscript;

704 Sina Saremi gave technical and scientific support during the implementation of the models, provided the code for the  
705 propellers modelization as input to MIKE and supported the writing and finalization of the manuscript;

706 Andrea Pedroncini first conceived the idea of the methodology adopted in the study, gave scientific support for the  
707 implementation of the models and feedback during the writing of the manuscript;

708 Jacob H. Jensen provided scientific support and advice regarding the driving mechanisms of naval induced sediment  
709 dynamics;

710 Silvia Torretta provided technical support for the model implementation and for the observed bathymetry analysis and  
711 reconstruction;

712 Caterina Vincenzi and Marco Vaccari provided bathymetry data, sediment data and information on dredging activities  
713 and general sediment related issues. They also favored the acquisition of the naval traffic data.

714

715 **Competing interests:**

716 Caterina Vincenzi and Marco Vaccari are employees of the Port Authority of Genova (Autorità di Sistema Portuale del  
717 Mar Ligure Occidentale), which commissioned and funded the present study to DHI, a private not-for-profit  
718 consultancy and research company in the field of water. Andrea Pedroncini, Silvia Torretta, Sina Saremi and Jakob H.  
719 Jensen are DHI employees. Antonio Guarnieri was DHI employee when the study was conducted; he is now employed  
720 at Istituto Nazionale di Geofisica e Vulcanologia (INGV).

721

722 **Acknowledgments**

723 We are grateful to Stazioni Marittime SpA for providing the daily traffic data of the Port of Genoa which was the  
724 starting point for this study. We are particularly grateful to Captain Calcagno of Stazioni Marittime SpA for the  
725 qualified and experienced information he gave on the sediment and vessels' dynamics in the port, which helped set up  
726 the numerical models, interpret and rely on the final results.

727 We are also particularly grateful to both the anonymous referees who revised the first version of the manuscript since  
728 their constructive critique and comments helped us enrich and improve the final version of the article.

729

730 **References**

- 731 • Abromeit, U., Alberts, D., Fischer, U., Fleischer, P., Fuehrer, M., Heibaum, M., Kayser, J., Knappe, G.,  
732 Köhler, H.J., Liebrecht, A., Reiner, W., Schmidt-vöcks, D., schulz, H., Schuppener, B., Söhngen, B., Soyeaux,  
733 R.: Principles for the Design of Bank and Bottom Protection for Inland Waterways, 1st Edition, Bundesanstalt  
734 für Wasserbau, Karlsruhe, 2010.
- 735 • Amorim, J.C.C., Bundgaard, K. and Elfrink, B.,: Environmental impact assessment of dredging deep in the  
736 navigation channel of the Port of Santos. In Environmental Hydraulics, Two Volume Set (pp. 639-644). CRC  
737 Press, 2010
- 738 • Castells-Sanabra, M., Mujal-Colilles, A., LLull, T., Moncunill, J., Martínez de Osés, F., & Gironella, X.  
739 (2020). Alternative Manoeuvres to Reduce Ship Scour. Journal of Navigation, 1-18.  
740 doi:10.1017/S0373463320000399
- 741 • Ciccacci, S., D'Alessandro, L., Fredi, P., and Lupia Palmieri, E. (1989). Contributo dell'analisi geomorfica  
742 quantitativa allo studio dei processi di denudazione nel bacino idrografico del Torrente Paglia (Toscana  
743 meridionale - Lazio settentrionale),Suppl. Geogr. Phys. Dinam. Quat., I, 171-188,  
744 <https://doi.org/10.13140/2.1.2991.6802>, 1989.
- 745 • CIRIA, CUR, CETMEF: The Rock Manual. The use of rock in hydraulic engineering, 2nd edition, C683  
746 CIRIA, London, 2007.
- 747 • DHI: MIKE 3 Flow Model HD FM - Hydrodynamics Flexible Mesh - Scientific Documentation, DHI,  
748 Hørsholm, 2017.
- 749 • DHI: MIKE 3 MT FM - Mud Transport Flexible Mesh - Scientific Documentation, DHI, Hørsholm, 2019.
- 750 • Flather, R.: A tidal model of the northwest European continental shelf, Memories de la Societe Royale des  
751 Sciences de Liege, 6, 10, 141–164, 1976.

- 752 • Grabe, J., Van Audgaerden, T., Busjaeger, D., Gerrit de Gijt, J., Heibaum, M., Heimann, S., Van der Horst, A.,  
753 Kalle, H.U, Krenzel, R., Lamberts, K.H., Miller, C., Morgen, K., Peshken, G., Retzlaff, T., Reuter, E.,  
754 Richwein, W., Ruland, P., Schrobenhausen, W. S., Tworushka, H., Vollstedt, H.W.: Recommendations of the  
755 Committee for Waterfront Structures, Harbours and Waterways - EAU 2012, 9<sup>th</sup> Edition, Issued by the  
756 Committee of Waterfront Structures of the German Port Technology Association and the German Geotechnical  
757 Society, Ernst & Sohn GmbH & Co., Berlin, 661, 2015.
- 758 • Grant W. and Madsen O.: Combined wave and current interaction with a rough bottom, *J. Geophys. Res.*, 84,  
759 1797–1808, 1979.
- 760 • Hamill, G.A.: Characteristics of the screw wash of a maneuvering ship and the resulting bed scour, Ph.D.  
761 dissertation, Queen’s Univ. of Belfast, Belfast, Northern Ireland, 1987.
- 762 • Hamill, G. A., Johnston, H. T., Stewart, D. P.: Propeller Wash Scour near Quay Walls, *Journal of Waterway,*  
763 *Port, Coastal, and Ocean Engineering*, 170-175, V 125, 4, [https://doi.org/10.1061/\(ASCE\)0733-](https://doi.org/10.1061/(ASCE)0733-950X(1999)125:4(170))  
764 [950X\(1999\)125:4\(170\)](https://doi.org/10.1061/(ASCE)0733-950X(1999)125:4(170)), 1999
- 765 • Hong, J. H., Chiew, Y.M, Hsieh, S. C., Cheng, N.S., and Yeh, P.H.: Propeller Jet–Induced Suspended-  
766 Sediment Concentration, *J. of Hydraul. Eng.*, 142, 2, [https://doi.org/10.1061/\(ASCE\)HY.1943-7900.0001103](https://doi.org/10.1061/(ASCE)HY.1943-7900.0001103),  
767 2016.
- 768 • Kristensen, H. O.: Analysis of technical data of Ro-Ro ships, in: Report n. 02 - of Project n. 2014-122  
769 Mitigating and reversing the side-effects of environmental legislation on Ro-Ro shipping in Northern Europe,  
770 HOK Marineconsult ApS, 2016.
- 771 • Krone, R.: Flume studies of the transport of sediment in estuarial processes: Final Report, Hydraulic  
772 Engineering Laboratory and Sanitary Engineering Research Laboratory, Univ. of California, Berkely, 1962.
- 773 • Lam, W., Hamill, G., Robinson, D., Raghunathan, R., and Kee, C., Submerged propeller jet, WSEAS  
774 Conferences, Udine, Italy, 20-22 January 2005.
- 775 • Leonard, B.P.: The ULTIMATE conservative difference scheme applied to unsteady one-dimensional  
776 advection, *Comput. Method Appl. M.*, 88, 17-74, [https://doi.org/10.1016/0045-7825\(91\)90232-U](https://doi.org/10.1016/0045-7825(91)90232-U), 1991.
- 777 • Lisi, I., Feola, A. , Bruschi, A., Di Risio, M., Pedroncini, A., Pasquali, D., and Romano, E.: La modellistica  
778 matematica nella valutazione degli aspetti fisici legati alla movimentazione dei sedimenti in aree marino-  
779 costiere, *Manuali e Linee Guida ISPRA*, 169/2017, 144., 2017.
- 780 • MarCom Working Group 180: PIANC REPORT N° 180 - Guidelines for Protecting Berthing Structures from  
781 Scour Caused by Ships, PIANC Secrétariat Général., Bruxelles, 2015.

- 782 • Mujal-Colilles, A., Gironella, X., Sanchez-Arcilla, A., Puig Polo, C., and Garcia-Leon, M.: Erosion caused by  
783 propeller jets in a low energy harbour basin, *J. Hydraul. Eng.*,  
784 <https://doi.org/10.1080/00221686.2016.1252801>, 2016.
- 785 • Mujal-Colilles, A., Castells, M., Llull, T., Gironella, X., Martínez de Osés, X.: Stern Twin-Propeller Effects on  
786 Harbor Infrastructures. Experimental Analysis. *Water* 2018, 10, 1571.
- 787 • Parchure, T., and Metha, A.: Erosion of soft cohesive sediment deposits, *J. of Hydraul. Eng.*, 111, 10, 1308-  
788 1326, [https://doi.org/10.1061/\(ASCE\)0733-9429\(1985\)111:10\(1308\)](https://doi.org/10.1061/(ASCE)0733-9429(1985)111:10(1308)), 1985.
- 789 • Partheniades, E.: Erosion and deposition of cohesive soils, *Journal of the Hydraulics Division*, 91, 105-139,  
790 1965.
- 791 • Rapaglia, J., Zaggia, L., Ricklefs, K. , Gelinas M., and Bokuniewicz, H.: Characteristics of ships' depression  
792 waves and associated sediment resuspension in Venice Lagoon, Italy: *J. Marine Syst.*, 85, 45-56,  
793 <https://doi.org/10.1016/j.jmarsys.2010.11.005>, 2011.
- 794 • Sanford, L.P. and Maa, J.P.Y.: A unified erosion formulation for fine sediments. *Marine Geology*, 179 (1-2),  
795 pp.9-23, 2001
- 796 • Soulsby, R., Hamm, L. , Klopman, G., Myrhaug, D., Simons, R., and Thomas, G.: Wave-current interaction  
797 within and outside the bottom boundary layer, *Coast. Eng.*, 21, 41-69, 1993.
- 798 • Teeter, A.: Vertical transport in fine-grained suspension and nearly-deposited sediment, in: *Estuarine Cohesive*  
799 *Sediment Dynamics*, 14, Mehta, A.J., Springer Verlag, 126-149, <https://doi.org/DOI:10.1029/LN014>, 1986.
- 800 • Teisson, C., Ockenden, M., Le Hir, P., Kranenburg, C. and Hamm, L.: Cohesive sediment transport  
801 processes. *Coastal Engineering*, 21(1-3), pp.129-162, 1993
- 802 • UNESCO, The practical salinity scale 1978 and the international equation of state of sea water, UNESCO  
803 *Technical Papers in Marine Science* 36, 25 pp.,1981a."
- 804 • Van Rijn, L.: Unified view of sediment transport by currents and waves. Initiation of motion, bed roughness,  
805 and bed-load transport, *J. Hydraul. Eng.*, 133, 6, 2007.
- 806 • Verhei, H. J.: The stability of bottom and banks subjected to the velocities in the propeller jet behind ships, 8th  
807 *International Harbour Congress*, Antwerp, June 13-17, 303, 1983.
- 808 • Winterwerp, J., and Van Kesteren, W.: *Introduction to the Physics of Cohesive Sediment in the Marine*  
809 *Environment*, 1st Edition, 56, Elsevier B.V., Amsterdam, 576, 2004.
- 810 • Yuksel, Y., Tan, Y., Celikoglu, Y.: Determining propeller scour near a quay wall. *Oc. Eng.*, 188, 2019.